Site U1400[1]

Expedition 340 Scientists[2]

Chapter contents

Background and objectives

Integrated Ocean Drilling Program (IODP) Site U1400 (proposed Site CARI-07C; 14°32.58′N, 61°27.55′W; 2745 meters below sea level [mbsl]) is located west of Martinique (Fig. F1). Site U1400 was dedicated to the study of debris avalanche emplacement and associated erosional processes. The evolution of the active Montagne Pelée Volcano is characterized by three major flank-collapse events (~0.1 m.y., ~25,000 y, and ~9000 y ago) that systematically destroyed the western flank of the volcano (Le Friant et al., 2003; Boudon et al., 2005, 2007). The volume of material displaced by these collapses varies from 2 to 25 km^3, with the debris avalanches depositing into the Grenada Basin. The Pitons du Carbet Volcano experienced a sector collapse 0.3 m.y. ago (Boudon et al., 1992, 2007; Samper et al., 2007). As shown by bathymetric and seismic data obtained during several site surveys, drilling to 510 meters below seafloor (mbsf) would penetrate through volcanic and biogenic sediment with intercalated large chaotic units (interpreted as debris avalanche Deposits 1 and 2). Of particular interest are the contacts between the different units, not only to distinguish between the different deposits but also to better understand mass transport dynamics, especially in the basal part of the flow. This study will provide fundamental constraints on friction parameters needed for realistic avalanche propagation models. Sediment above the deposit will be dated using $\delta^{18}O$ chronostratigraphy to better constrain the age of this event. As shown on the seismic profiles, a thick and well-bedded sedimentary layer (~70 m) overlies Deposit 2 with an abnormal thickness toward the northeast. We will test the hypothesis that, following a flank collapse, the on-land drainage system is drastically modified, resulting in increased erosion and, therefore, increased sedimentation rates in the Grenada Basin.

Operations

Transit to Site U1400

After pulling thrusters at Site U1399, the vessel switched to cruise mode and began the 17 nmi move to Site U1400. The vessel stabilized over Hole U1400A at 1625 h on 4 April 2012. All times reported in this volume are given in ship local time, which was Universal Time Coordinated (UTC) – 4 h. The position reference was a combination of GPS signals and one of two acoustic beacons. The first positioning beacon was deployed at 1650 h on 4 April

[1] Expedition 340 Scientists, 2013. Site U1400. *In* Le Friant, A., Ishizuka, O., Stroncik, N.A., and the Expedition 340 Scientists, *Proc. IODP,* 340: Tokyo (Integrated Ocean Drilling Program Management International, Inc.). doi:10.2204/iodp.proc.340.110.2013
[2] **Expedition 340 Scientists' addresses.**

doi:10.2204/iodp.proc.340.110.2013

~250 m from the primary site coordinates along the seismic line running to the northeast in anticipation of a move in that direction for Hole U1400B. The second beacon was deployed 250 m to the southeast along the crossing seismic line at 1410 h on 5 April. At the end of operations at Site U1400, both beacons were sent acoustic commands to release. The first beacon was retrieved at 0500 h on 13 April, but the second beacon apparently did not release and was not recovered. The vessel began a dynamic positioning move to the next site at 0630 h on 13 April.

Site U1400

Site U1400 consists of three holes (Table T1). The original plan called for two holes to be cored to ~510 mbsf. The first hole was terminated at 51.3 mbsf because of unstable hole conditions. After offsetting the vessel 750 m in a direction 160° from Hole U1400A, the second hole, U1400B, was piston cored to 212.5 mbsf. After the core barrel became stuck, the drill string had to be tripped to the surface and the core barrel freed from the upper landing sub. A shear pin had become wedged between the removable landing seat and the core barrel assembly. After offsetting 20 m further along the 160° seismic line, the third hole of the site began with two failed attempts at spudding Hole U1400C. The first failed attempt broke off the lower section of a nonmagnetic core barrel with the cutting shoe. After the core barrel was retrieved and the breakage was discovered, a steel core barrel was installed and run to bottom. The second attempt was even less successful. This time the steel barrel bent in such a fashion that it was unable to be pulled back through the bottom-hole assembly (BHA). The drill string was again pulled to surface, and the bent core barrel was cut away and the BHA was reassembled for another attempt. This time, the hole was advanced to 15 mbsf without coring before running in with the wireline to begin coring. Coring with the advanced piston corer (APC) continued through Core 340-U1400C-22H at 191.1 mbsf. APC coring was terminated when the formation became so stiff that the core liner folded up inside the core barrel and had to be pumped out with a 10,000 psi pump. The extended core barrel (XCB) was then deployed and used to successfully complete coring operations to 436 mbsf. A logging program was planned for Hole U1400C; however, hole problems, resulting in a severed BHA, forced the abandonment of the hole. The vessel was then moved 7 nmi to Site U1401 using the dynamic positioning system. The APC was deployed 58 times. The cored interval with the APC was 439.9 m with a recovery of 447.34 m of core (102%). The XCB coring system was deployed 27 times. The cored interval with the XCB system was 244.9 m with a recovery of 124.14 m of core (51%). Overall recovery for Site U1400 was 83%. Total time spent on Site U1400 was 207.00 h.

Hole U1400A

The vessel arrived at Site U1400 and was in position at 1630 h on 4 April 2012. The pipe trip to bottom was uneventful. The top drive was then picked up, and the bit was spaced out to spud Hole U1400A. The initial corrected precision depth recorder (PDR) reading was 2755.4 meters below rig floor (mbrf). The bit was set at 2750 mbrf, and the hole was spudded at 0030 h on 5 April. The seafloor depth was calculated from the length of the first core (3.5 m) to be 2756.0 mbrf (2744.4 mbsl). The APC was advanced to Core 340-U1400A-9H at 51.3 mbsf. Apart from the first core, all piston strokes were partial strokes. Eight partial strokes were recorded. The hole was advanced by recovery. At 51.3 mbsf, the drill string became stuck without circulation and rotation. Keeping within the overpull limits, the string was worked and was eventually freed from the formation. The decision was made to abandon Hole U1400A and offset the vessel as far as beacon deployment would allow. Nine piston cores were taken over the 51.3 m interval with a total recovery of 51.8 m of core (101%). The drill string was pulled clear of the seafloor at 1445 h on 5 April, ending Hole U1400A. Total time spent on Hole U1400A was 22.25 h.

Hole U1400B

Because of challenging hole conditions, we decided to move Hole U1400B as far away from Hole U1400A as possible. A second beacon was deployed 250 m on a heading of 160° from Hole U1400A. We decided to maximize beacon-offset capabilities, and the final distance between Holes U1400A and U1400B was 750 m at a heading of 160°. Hole U1400B was spudded at 1605 h on 5 April 2012. Seafloor depth was calculated from the length of the first core (6.8 m) to be 2754.7 mbrf (2743.0 mbsl). APC coring advanced to Core 340-U1400B-28H at 213 mbsf. Twelve partial APC strokes were recorded—most near the top section of the hole. The hole was advanced by recovery. After shooting Core 28H, we were unable to pull the core barrel to surface. Two wireline runs were made to attempt to free the core barrel. After the second attempt, we abandoned Hole U1400B and retrieved the BHA to free the stuck core barrel. Twenty-eight APC cores were taken from 0 to 212.5, recovering 215.19 m of core (101%). The drill string was pulled back to the rig floor, and the core barrel was extricated from the BHA. A shear pin had become lodged between the landing seat and the core barrel assembly. The landing seat had to be removed from the landing sub and cut off with an acetylene torch. After

removing all the coring equipment from the BHA, Hole U1400B ended at 1030 h on 7 April. The total time spent on Hole U1400B was 43.75 h.

Hole U1400C

We decided a third hole was necessary to fully achieve the science objectives of Site U1400. The vessel was offset another 20 m at 160° from Hole U1400B. After tripping to bottom, the bit was set at 2751 mbrf. A mudline core was attempted, but the bottom section of the nonmagnetic core barrel broke off. Because the uppermost 20–25 mbsf of Hole U1400B had been hard sand, we switched to steel core barrels to make another attempt at a mudline core. Despite successfully coring the mudline on Hole U1400B, the second mudline core attempt in Hole U1400C resulted in a bent core barrel. Because we could not pull the core barrel out of the BHA, the entire drill string had to be tripped back to surface. After the BHA reached the rig floor, it was necessary to remove the bit and bit sub and to cut the steel barrel so that it could be pulled back through the bottom of the BHA.

The BHA was reassembled and tripped back to just above the seafloor. We then picked up the top drive to spud Hole U1400C at 0950 h on 8 April 2012. The seafloor depth of Hole U1400C was assumed to be the same as at Hole U1400B: 2754.7 mbrf (2743.0 mbsl). To penetrate through the problematic seafloor surface, we drilled without coring from 0 to 15 mbsf. APC coring started with Core 340-U1400C-2H at 15 mbsf. Advanced piston corer temperature tool (APCT-3) measurements were taken on Cores 5H, 8H, and 12H. Core orientation started on Core 5H, and nonmagnetic core barrels were deployed starting with Core 2H. Because of poor hole conditions, the core orientation tool and the nonmagnetic core barrels were not used after Core 10H. Ten out of twenty-two piston cores were partial strokes, and the hole was therefore advanced by recovery. After reaching APC refusal on Core 22H, the XCB was deployed and XCB coring continued to 436.0 mbsf. Coring was terminated after Core 49X. Twenty-one piston cores were taken over a 176.1 m interval with a total recovery of 180.35 m of core (102%). Twenty-seven XCB cores were taken over a 244.9 m interval. A total of 124.14 m of core were recovered (51%), and the hole was terminated at 436.0 mbsf. Overall core recovery for Hole U1400C was 72%.

At the conclusion of coring, Hole U1400C was conditioned with a 25 bbl high-viscosity mud sweep and displaced with 201 bbl of 10.5 ppg mud. While attempting to pull out of the hole to logging depth, the drill string started to pick up overpull between 400 and 320 mbsf. By the time the bit had reached 318 mbsf, upward motion of the drill string was almost impossible. For almost 17 h, we attempted to backream the BHA upward. At 0045 h on 12 April, we effectively lost rotation but not circulation. After trying to free the stuck pipe, the Schlumberger Wireline Engineer was called out to rig up the severing charges. At 0945 h, the first severing charge was used to sever the drill string at the top of the tapered drill collar. After the charge was detonated, we were still unable to establish rotation or upward movement of the drill string. A second severing charge was prepared and run in the hole with the Schlumberger wireline to just below the seafloor. At 1845 h we attempted to detonate and were still unable to free the pipe. On removal of the tool from the pipe, the charge was found to be intact. No detonation had occurred. Several hours were spent troubleshooting the tool at the surface and, after finding a faulty connection, the tool was reassembled and run back to bottom. Shortly after midnight on 13 April, the drill string was severed and rotation and upward movement were reestablished. The entire BHA, including two stands of 5½ inch drill pipe and 15 joints of 5 inch drill pipe, was abandoned in Hole U1400C. The remainder of the pipe was tripped to the surface, and the severed joint of drill pipe cleared the rotary table at 0730 h on 13 April, ending Hole U1400C and Site U1400. Total time spent on Hole U1400C was 141.0 h.

Lithostratigraphy

Three holes were drilled at Site U1400. Correlations can be established between Holes U1400A and U1400B in the uppermost tens of meters and between Holes U1400B and U1400C between 15 and 213.4 mbsf (213.4 mbsf is the base of Hole U1400B). Figure **F2** summarizes the correlations between units in all three holes.

Site U1400 sediment was divided into seven lithostratigraphic units (A–G). Overall, the hole is dominated by a combination of hemipelagic mud with interbedded tephra layers, volcaniclastic turbidites, and deformed sediment. Units A–G consist of varying proportions of these lithologies. Each lithology is described in detail in **"Lithostratigraphy"** in the "Site U1394" chapter (Expedition 340 Scientists, 2013b), and the deformed sediment is described in **"Lithostratigraphy"** in the "Site U1398" chapter (Expedition 340 Scientists, 2013c).

Unit A

Depths: Hole U1400A = 0–27 mbsf, Hole U1400B = 0–2.94 mbsf

Unit A extends from 0 to 27 mbsf in Hole U1400A and from 0 to 2.94 mbsf in Hole U1400B. In Hole

U1400C, core recovery began at 15 mbsf, so Unit A is not observed. Unit A can be divided into three subunits (A-1 to A-3).

Subunit A-1

Subunit A-1 is thin, measuring 16 cm in Hole U1400A and 5 cm in Hole U1400B. It consists of dark gray massive volcanic sand. It can probably be associated with the last historic 1902–1905 and 1929–1932 dome-forming eruptions of Montagne Pelée, as they are the upper deposits in the core. These deposits contain pumice that is not found in dome-forming eruptions. As such, they cannot be interpreted as primary deposits but are more likely reworked material that includes older pumiceous deposits.

Subunit A-2

Subunit A-2 measures 14 cm in Hole U1400A and 23 cm in Hole U1400B; it consists of oxidized brown hemipelagic mud with high water content. This subunit is generally found at the top of the core in the other holes, as no historic deposits occur above it.

Subunit A-3

Subunit A-3 extends from 0.3 to 27 mbsf in Hole U1400A and from 0.3 to 2.94 mbsf in Hole U1400B. This subunit is composed of alternating layers of hemipelagic mud, tephra, and turbidites. Pumice is present in all the deposits, ranging from <5% to >60%. Scoria was also identified in some of the tephra layers. This subunit is considerably thinner in Hole U1400B than it is in Hole U1400A.

Unit B

Depths: Hole U1400A = 27–51.3 mbsf (bottom of hole), Hole U1400B = 2.94–25.5 mbsf, Hole U1400C = 15–22 mbsf

Unit B extends from 27 to below 51 mbsf in Hole U1400A, from 2.94 to 25.5 mbsf in Hole U1400B, and from 15 to 22 mbsf in Hole U1400C. Unit B is composed of thick volcaniclastic sand with no hemipelagic sediment or tephra layers interbedded. Both pumice and scoria were found as clasts in this unit. The base of this unit is not observed in Hole U1400A because the hole was terminated at 51 mbsf.

Unit C

Depths: Hole U1400B = 25.5–35 mbsf, Hole U1400C = 22–24.8 mbsf

Unit C extends from 25.5 to 35 mbsf in Hole U1400B and 22 to 24.8 mbsf in Hole U1400C. Unit C is dominantly composed of mottled gray-green hemipelagic mud with several tephra layers and two thin turbidites. Pumice is abundant in both the tephra layers and the turbidites; some of the layers contain as much as 90% pumice. Hemipelagic mud accounts for >90% of this unit. Green laminae containing glauconite frequently occur in the hemipelagic mud interval.

Unit D

Depths: Hole U1400B = 35–58 mbsf, Hole U1400C = 24.8–59 mbsf

Unit D extends from 35 to 58 mbsf in Hole U1400B and from 24.8 to 59 mbsf in Hole U1400C. From the top of Unit D to the base of Unit F (212.5 mbsf in Hole U1400B; 390 mbsf in Hole U1400C), the core material consists of more or less deformed sediment with interbedded tephra layers and, in a few places, turbidites. Deformation is principally identified by inclined tephra layers, inclined contacts between turbidites and hemipelagic mud, and inclined glauconite-rich green laminae in the hemipelagic mud. Inclination can be shallow (a few degrees) to high (≤80°). No debrites are observed in this thick sequence of sediment in Hole U1400B, and only a few debrite intervals are observed in Hole U1400C. This paucity of debrites contrasts with the more frequent debrite intervals seen in cores from Site U1399.

Unit D is composed of gray mud and, in some places, highly mottled gray-green-brown mud with interbedded tephra layers (and a few turbidites in Hole U1400C). With the exception of the uppermost 3 mbsf in Hole U1400B, where the inclination of layers is high (60°–70°), most of the sediment is weakly deformed (inclined at 20°) or contorted. Despite a relatively shallow present-day burial depth, the sediment is occasionally highly indurated (see **"Physical properties"**). Green laminae are abundant and help show the deformation of the sediment. Most tephra layers contain pumice in various proportions. The few turbidites that are observed in Hole U1400C contain as much as 60% pumice.

Unit E

Depths: Hole U1400B = 58–212.5 mbsf, Hole U1400C = 59–190 mbsf

Unit E extends from 58 to 212.5 mbsf in Hole U1400B and from 59 to 190 mbsf in Hole U1400C. Unit E is divided into three subunits (E-1 to E-3) based on the proportion of volcanic layers interbedded with the hemipelagic mud and by the intensity of the deformation.

Subunit E-1

In Subunit E-1 (58–67 mbsf in Hole U1400B; 59–76 mbsf in Hole U1400C), deformation is more intense than it is in Unit D, with beds inclined at an

average of 40°. This subunit contains a high proportion of tephra layers (for example, 33 layers between 64.9 and 66.6 mbsf in Hole U1400B). Most of the tephra layers contain pumice, with proportions varying between 5% and 60%.

Subunit E-2

Subunit E-2 (67–111.6 mbsf in Hole U1400B; 76–101 mbsf in Hole U1400C) contains primarily hemipelagic mud with many interbedded tephra layers and numerous turbidites that range in thickness from a few tens of centimeters to several meters. As with previous units, turbidites contain a significant amount of pumice. In general, the sediment is weakly deformed, with most of the tephra layers featuring subhorizontal contacts. A 2 m thick, pink-colored volcanic ash rich in pumice and glass shards (75%) is observed in Hole U1400C at 82.4–84.5 mbsf. The ash forms a good reference layer that is also observed in Hole U1400B at 84 mbsf, where it appears to be thinner.

Subunit E-3

Subunit E-3 (111.6–212.5 mbsf in Hole U1400B; 101–190 mbsf in Hole U1400C) is generally composed of highly deformed hemipelagic sediment with steeply inclined (≤70°) contacts. Only a few zones of weakly deformed hemipelagic mud are included. As with Subunit E-2, there are abundant tephra layers and many of them contain pumice. Only a few volcaniclastic turbidites are present in Hole U1400C, whereas a 2.3 m thick mixed (bioclastic-volcaniclastic) turbidite is observed in Hole U1400B that contains a large proportion of mud clasts.

Units F and G

Units F and G are only observed in Hole C. They are composed of highly indurated sediment that becomes progressively more lithified with depth, eventually occurring as mudstone.

Unit F

Depth: Hole U1400C = 190–390 mbsf

Unit F extends from 190 to 390 mbsf in Hole U1400C. This unit is composed of a succession of deformed (and lithified) hemipelagic sediment. The inclination of bedding and contacts is ≤80°. The unit locally contains many tephra layers. In some sections, hemipelagic mud is mixed with volcanic sand, attesting to the important deformation and mixing of the sediment and volcanic layers. Unit F represents probably the most highly deformed part of the hole. A few muddy sand debrite intervals, frequently rich in pumice clasts, are observed at different depths within the unit.

Unit G

Depth: Hole U1400C = 390–436 mbsf

Unit G extends from 390 to 436 mbsf in Hole U1400C. The top of Unit G marks the lower boundary of the deformed sediment, below which only flat-lying hemipelagic muds and partly lithified mudstones are found. The sediment lacks inclined contacts or green laminae. Two small pumice-rich debrite layers are observed in the upper part of Unit G.

Paleontology and biostratigraphy

Core catcher samples at Site U1400 contain calcareous nannofossils and planktonic and benthic foraminifers of varying abundances. The consistency of the sediment within the core catcher samples varied between loose and highly indurated, particularly at the base of Hole U1400C. Calcareous nannofossil and planktonic foraminiferal data both suggest late Pleistocene ages (Fig. **F3**) for the majority of the samples. However, near or at the base of each hole, species indicative of older material are present (see Fig. **F4** for a summary). Major to minor reworking is evident throughout Site U1400. Because of both the reworking and the presence of substantial mass-flow deposits, a calculated sedimentation rate would be grossly misleading.

Calcareous nannofossils

Samples from Site U1400 are mainly composed of late Pleistocene sediment, changing to late Pliocene sediment at the base of Hole U1400C. Only five core catcher samples from Hole U1400A were analyzed for nannofossils because of the coarse nature of the material collected. For Holes U1400B and U1400C, the sediment collected was generally finer grained. A total of 20 core catcher samples were analyzed for Hole U1400B, and 41 core catcher samples were analyzed for Hole U1400C. In Holes U1400A and U1400B, the uppermost core catcher samples (340-U1400A-1H-CC and 2H-CC and 340-U1400B-2H-CC) contained common *Gephyrocapsa* sp., but >90% of the assemblage consisted of small 2–3 µm forms presumed to be *Emiliania huxleyi*, which would indicate an age younger than 84 ka within Zone CN15 (Okada and Bukry, 1980). Reworked discoasters and *Sphenolithus abies/neoabies* species were observed in Sample 340-U1400A-2H-CC. Specimens within the genus *Discoaster* are heavily overgrown and could not be identified to species level. However, Sample 340-U1400A-7H-CC contains a variety of reworked discoaster species such as *Discoaster surculus*, *Discoaster brouweri*, and *Reticulofenestra umbilicus*, along with

late Pleistocene species. In general, background sedimentation in Hole U1400A was assigned to Zone CN15 (Okada and Bukry, 1980).

Core catcher samples (340-U1400B-2H-CC and 28H-CC) from Hole U1400B contain abundant *E. huxleyi*, *Gephyrocapsa parallela*, *Gephyrocapsa oceanica*, *Ceratolithus cristatus*, and small *Gephyrocapsa* species (<2.5 µm). These samples were assigned to Zone CN15 (Okada and Bukry, 1980). *Pseudoemiliania lacunosa* was common in both Holes U1400A and U1400B; however, they were observed to be reworked. Hole U1400C is similar to Hole U1400B in terms of biostratigraphic nannofossil zonation. Because of the high occurrence (abundant to few) of *E. huxleyi*, *Gephyrocapsa* sp., *C. cristatus*, *Ceratolithus telesmus*, and *Ceratolithus simplex*, Samples 340-U1400C-2H-CC to 36X-CC were assigned to Zone CN15. At the bottom of Hole U1400C, many samples did not provide reliable age markers because of poor preservation. *Gephyrocapsa* sp. and *E. huxleyi* are largely absent in Samples 340-U1400C-39X-CC, 40X-CC, 41X-CC, 43X-CC, and 44X-CC. However, Samples 340-U1400C-45X-CC to 49X-CC yielded a characteristic upper Pliocene assemblage of *D. brouweri*, *D. surculus*, *Calcidiscus macintyrei*, and *Discoaster asymmetricus*. These samples correlate with Zone CN12 (Kameo and Bralower, 2000).

Planktonic foraminifers

All core catcher samples from Holes U1400A, U1400B, and U1400C (9, 28, and 49 samples, respectively) were analyzed for planktonic foraminiferal content. Planktonic foraminifers are present in most of the analyzed samples but are absent in Samples 340-U1400A-6H-CC, 340-U1400B-4H-CC and 9H-CC, and 340-U1400C-9HCC, 24X-CC, and 30X-CC, possibly because of the high volume of volcanic material in these samples. In samples with abundant specimens, the assemblage of planktonic foraminifers is diverse but dominated by *Globigerinoides ruber* (white and pink), *Globigerinoides sacculifer*, and *Neogloboquadrina dutertrei* (dextral). Other abundant species include *Pulleniatina obliquiloculata* and *Sphaeroidinellopsis dehiscens*. In all holes, the population changes toward the base, reflecting a likely Pliocene assemblage. This change is most obvious in Hole U1400C; in Sample 340-U1400C-36X-CC, *P. obliquiloculata* is reduced in number, and absent in Sample 38X-CC, whereas *Globorotalia miocenica* and *Globorotalia exilis* become more abundant. All these changes reflect an upper Pliocene rather than a lower Pleistocene foraminiferal assemblage. All species present are indicative of warm subtropical waters.

Several datum species were found in all three holes. The most frequently encountered datum species was *Globigerinella calida* (bottom occurrence at 0.22 Ma), which was found in low numbers throughout most of each hole. A further late Pleistocene marker, *Globorotalia flexuosa* (0.07–0.40 Ma), was only found in three samples (340-U1400B-22H-CC and 340-U1400C-19H-CC and 20H-CC). The co-occurrence of *Globorotalia tosaensis* (top occurrence [T] at 0.61 Ma), which does not have an overlapping range with either *G. calida* or *G. flexuosa*, indicates reworking through a large portion of the late Pleistocene sediments. At the base of Hole U1400A (Sample 340-U1400A-7H-CC), Hole U1400B (Sample 340-U1400B-28H-CC), and Hole U1400C (Samples 340-U1400C-33X-CC to 49X-CC), *G. miocenica* (T 2.39 Ma) is abundant and, without any conflict from a younger species, most likely reflects the true age of sediments. This suggests a large gap of >2 m.y. Other late Pliocene markers present include *Globigerinoides extremus* (T 1.99 Ma) and *G. exilis* (T 2.10 Ma), further corroborating the PL5 zonation. The early Pliocene marker species *Globorotalia cibaoensis* (T 4.60 Ma) was also found in low numbers throughout the late Pliocene sediments in Hole U1400C, though it appears to be reworked.

Figure F4 summarizes the occurrences of important planktonic foraminifer species and highlights the extent to which reworking was apparent within the three holes. It should be noted that in Hole U1400C, the bottom contact of the reworked *G. tosaensis* is not well defined, as both preservation and abundance deteriorate for ~40 m below its lowest occurrence and no specimens are found within those samples. This may help to explain the seemingly impossible relationship of *G. tosaenesis* and *G. flexuosa* between Holes U1400B and U1400C.

Benthic foraminifers

A total of 31 genera and 26 species were identified at Site U1400 in the >150 µm size fraction. Benthic foraminifers examined in Holes U1400A, U1400B, and U1400C have very low abundances. Preservation varies from poor to very good. Ten species are present in Hole U1400A, fourteen in Hole U1400B, and sixteen in Hole U1400C. Overall, the abundance of specimens per species is very low (1–5 per sample) in most samples. Rotaliids have a very low diversity mainly represented by *Amphistegina*, *Cibicides wuellerstorfi*, *Melonis* sp., and *Osangularia* sp. Miliolids are present; *Pyrgo murrhina* and *Quinqueloculina granulocostata* are the more dominant species in all holes. Agglutinated foraminifers are extremely rare, with only *Sigmoilopsis* sp. present, and only in seven samples. Benthic foraminiferal abundance is low at Site U1400, ranging between 1 and 16 foraminifers/g of sediment with the exception of Sample 340-U1400B-7H-CC, which has an abundance of 33 foraminifers/g of sediment.

Pleurostomella alternans, *Siphonodosaria cooperensis*, *Siphonodosaria sargrinensis*, and *Siphonodosaria pomuligera* are present in very low abundances (1 specimen per sample) throughout Site U1400. Samples 340-U1400B-8H-CC, 14H-CC, 18H-CC, and 20H-CC contain relative higher abundances of *S. cooperensis* (≤10 individuals per sample). The top for this foraminiferal group is 0.58 Ma (Hayward et al., 2006).

The very low abundance of indicative species like *C. wuellerstorfi*, *P. murrhina*, and *Osangularia* sp. and the absence of other abyssal key taxa make it difficult to provide a reliable paleodepth estimate.

Geochemistry

Samples for headspace analyses were taken from 49 cores throughout all three holes at this site (Holes U1400A–U1400C). In contrast to the two previous sites (U1398 and U1399) in the basin, not a single sample had a methane concentration >4.1 ppm, and the vast majority had concentrations <3 ppm. No higher hydrocarbons were detected in any of the samples.

A total of 78 samples were taken for X-ray diffraction (XRD) and carbonate analysis at Site U1400. In general, the XRD patterns are very similar to those obtained from Sites U1398 and U1399. However, subtle variations in the relative proportions of volcanic minerals are present, with quartz and Fe-Ti oxides being more abundant than those seen at the deeper sites (Fig. **F5A**). Clay minerals were identified in virtually every sample and are present in high abundance (typically smectite, kaolinite, and glauconite) in some samples (Fig. **F5B**). As is typical in sediment cores taken near volcanic islands, carbonate concentrations are highly variable and are lower in intervals with higher proportions of volcanic material (Fig. **F6A;** Table **T2**). Maximum carbonate concentrations are ~35 wt%, reflecting the greater proportion of terrestrial clay minerals and the absence of significant aragonite preservation. An unusual aspect of the organic carbon data is a general increase in concentrations with depth (Fig. **F6B**). Concentrations in the upper 250 mbsf are generally low (mostly <0.5 wt%) compared to previous sites, whereas approximately half the samples from below this depth contain higher organic carbon concentrations, with some samples reaching 0.8 wt%.

Pore water profiles are illustrated in Figure **F7** and data are listed in Table **T3.** With the exception of the deepest sample from 427 mbsf, data can be readily interpreted in terms of a classic diagenetic profile driven by the oxidation of organic carbon (e.g., increasing alkalinity and ammonia and decreasing ΣS). Calcium and Mg data generally scatter near the seawater value with an increase in Ca and decrease in Mg in the deeper samples. Cl data show a steady increase in concentrations from the modern seawater value at the surface (560 mM) to 570 mM at 120 mbsf that likely reflects progressive hydration of altered volcanic material as it is altered to clay minerals. The chemical composition of the deepest sample deviates from this interpretation; in particular, it has a much lower ΣS concentration than the rest of the samples. This sample comes from much older sediment that appears to be separated from the younger overlying sediment by a hiatus of at least 1 m.y. (e.g., see **"Paleontology and biostratigraphy"**). The two deepest samples also contain the highest organic carbon concentrations. Hence, one interpretation of the data is that the pore water geochemistry of the deepest sample reflects a distinct diagenetic environment from that observed in the overlying sediment, which may either reflect changes in environmental conditions at this site over time or transport of the upper sediment to this area from a site of lower organic carbon deposition.

Physical properties

Good correlation exists between Holes U1400C and U1400B to ~200 mbsf. Analysis of the correlation suggests Hole U1400C has consistently thicker bedding than Hole U1400B. High magnetic susceptibility, *P*-wave velocity, and density values in the upper 20 mbsf correlate with higher sandy, volcanic content. *P*-wave velocity generally increases with depth, with the most significant variability in the uppermost 50 mbsf where we encountered coarse-grained volcaniclastic material. Shear strength measurements show significant variability with values generally increasing with depth. Temperature increases linearly with increasing depth in the uppermost 103 m with a temperature gradient of 52.9° ± 1.6°C/km.

Stratigraphic correlation between Holes U1400C and U1400B

Hole U1400A is shallow and distant from Holes U1400C and U1400B; we therefore only tied Holes U1400C and U1400B. We used both magnetic susceptibility and natural gamma radiation (NGR) data to correlate depths between the two holes (Fig. **F8**). We trimmed 5.1 cm off each end of core sections in the magnetic susceptibility data and 10 cm off each core section end in the NGR data to minimize edge effects during correlation. High core recovery in both holes resulted in robust correlation markers using both magnetic susceptibility and NGR. Hole U1400B was the reference hole for these correlations because it has the longest continuous record; however, both

holes have good, continuous recovery to ~230 mbsf. Except for the upper tens of meters, all correlation shifts for Hole U1400C are positive (upward). Several good correlation tie points exist between Holes U1400B and U1400C. Some of the tie points deeper than ~200 mbsf are offset by >20 m. This offset is unexpected because hole separation is ~20 m. Caution must therefore be used in the interpretation of deeper correlations. The most significant stretch between these holes occurs at 30–50 mbsf. At these depths, Hole U1400C requires a ~10 m upward shift for good correlation between holes. Below ~50 mbsf, Hole U1400C correlates well with Hole U1400B, and we applied only small upward shifts below 50 mbsf. Analysis therefore suggests that below 50 mbsf Hole U1400C has consistently thicker bedding than that found in Hole U1400B. We picked correlation points to ~200 mbsf with confidence. Below this depth, data are sparse and correlation picks are less reliable. Our correlation coefficient using both magnetic susceptibility data and NGR is 0.58. All picked correlation depth shifts are shown in Table **T4.**

Gamma ray attenuation density, magnetic susceptibility, and *P*-wave velocity

Changes in magnetic susceptibility correlate with lithologic changes. Where volcaniclastic sediment exists, magnetic susceptibility is high. In Hole U1400B, magnetic susceptibility reaches maximum values of 2500 × 10^{-5} SI between 0 and 25 mbsf and at 100 mbsf. In Hole U1400C, maximum values (~3000 × 10^{-5} SI) occur at 100 mbsf. At all locations where magnetic susceptibility values are high we see evidence for sandy volcanic turbidites. In hemipelagic sediment, magnetic susceptibility values remain low (mostly <400 × 10^{-5} SI). Bulk density also correlates with the cored material, showing high values (2.2 g/cm^3) in dense volcanic sands and low values (<1.7 g/cm^3) in hemipelagic sediment.

We measured higher *P*-wave velocities in volcaniclastic sediment (typically ~1750 m/s) in the upper 50 m of the holes and lower *P*-wave velocities in hemipelagic sediment. Where hemipelagic sediment dominates, *P*-wave velocity increases steadily with increasing depth.

Shear strength

Because of abundant sand in Hole U1400A, undrained shear strength (S_u) was measured discontinuously in fine-grained intervals within the uppermost 26 m (Cores 340-U1400A-1H through 5H) with the automated vane shear (AVS) and fall cone. S_u increases ~1 kPa/m with increasing depth.

In Holes U1400B and U1400C, S_u measurements were performed with the handheld penetrometer, fall cone, and AVS. Between 25 and 70 mbsf, S_u measurements with the handheld penetrometer and AVS increase ~4 kPa/m downhole, whereas S_u measurements with the fall cone are lower and increase ~1 kPa/m downhole. As a consequence, S_u values provided by the AVS are four times higher than those measured with the fall cone. The presence of sandy intervals between 70 and 105 mbsf leads to scattered S_u data and a relative decrease of S_u in the interbedded fine-grained sediment (as much as 50% for S_u from the handheld penetrometer). This decrease in S_u is in agreement with a relative decrease in GRA density and *P*-wave velocity.

Below 105 mbsf, S_u measurements from the handheld penetrometer exceed the measurement limit of the tool, indicating that shear strength is >220 kPa. Nevertheless, this increase in strength is not observed in fall cone measurements, which found that the residual strength of the sediment is constant downhole, with a mean value of ~40 kPa to 210 mbsf.

Sediment expansion observed during core cutting on the catwalk (Holes U1400B and U1400C) suggests that decompression reduces the S_u of the sediment substantially after retrieval. Measurements performed with the AVS and fall cone may therefore underestimate in situ conditions. On the other hand, S_u values provided by the handheld penetrometer are generally higher than those with the AVS and fall cone, with the fall cone providing the lowest S_u.

P-wave velocity

Discrete measurements of compressional wave velocity in hemipelagic mud match the general trend in values from the *P*-wave logger (PWL). Volcaniclastic sediment shows much higher velocities, ranging from 1700 to 1840 m/s. In Hole U1400C, from 210 to >400 mbsf, *P*-wave velocities in hemipelagic mud increase from 1650 to 1750 m/s and follow the PWL values.

Moisture and density

We collected 88 moisture and density (MAD) measurements (10 from Hole U1400A, 47 from Hole U1400B, and 38 from Hole U1400C), including 71 samples of hemipelagic sediment and 17 samples of volcaniclastic sand (turbidites).

Porosity of hemipelagic samples ranges between 51.5% and 73% (Figs. **F9, F10**). Like Site U1399, Site U1400 shows a weak negative porosity-depth correlation from ~66% at the mudline to ~60% at 427 mbsf. Volcanic sand samples have porosities between 36% and 51%. As at previous sites, porosity of loose sands may be underestimated because of draining of pore

water during sampling or overestimated because of sediment reworking during core recovery. Alternatively, where core recovery, handling, or splitting processes reorganize sand grains, sandy sediment may become undercompacted and yield anomalously high porosities.

Bulk density of hemipelagic samples ranges between 1.5 and 1.82 g/cm^3. Bulk density of sandy samples is as high as 2.18 g/cm^3, quite distinct from the densities of hemipelagic samples. Grain density of hemipelagic samples typically ranges between 2.53 and 2.77 g/cm^3. Volcanic sand has grain density between 2.74 and 2.87 g/cm^3, somewhat higher compared to that at Site U1399.

Thermal conductivity

Thermal conductivity was measured at 161 depths on recovered whole-round sections from all three holes. The measured thermal conductivity averaged 1.050 W/(m·K), with a standard deviation of 0.075 W/(m·K) and a standard error on the mean of 0.006 W/(m·K). There is a small but statistically significant increase of thermal conductivity with increasing depth (Manga et al., 2012).

Downhole temperature

Temperature was measured with the APCT-3 at the bottom of Cores 340-U1400C-5H, 8H, and 12H (48.3, 76.1, and 103.3 mbsf, respectively). Downhole temperature was monitored for 642, 645, and 2392 s, respectively. Temperature was calculated from these time series of temperature measurements using TP-Fit (see APCT-3 user manual on the Cumulus/Techdoc database at **iodp.tamu.edu/tasapps/**). We assume a thermal conductivity (k) of 1.0 W/(m·K) and $\rho C = 3.7 \times 10^6$ J/m^{3}K. To calculate uncertainty, we assume k ranges from 0.9 to 1.1 W/(m·K) and ρC is between 3.2×10^6 and 4.0×10^6 J/m^{3}K. At the base of Cores 340-U1400C-5H, 8H, and 12H, we obtained temperatures of 6.94° ± 0.03°C, 8.45° ± 0.03°C, and 9.68° ± 0.09°C, respectively. The uncertainties are greater than the error on the best-fit solution and the probe's measurement accuracy. The temperature of ocean water at the seafloor was 4.26°C.

A best-fit linear relationship between depth and our four temperature measurements gives a temperature gradient of 52.9° ± 1.6°C/km (Fig. **F11**). Using the measured thermal conductivity the implied heat flow is 56 ± 4 mW/m^2. The near-surface heat flow at this site, if conductive, is reduced 2% owing to bathymetry and as much as 4% because of sedimentation (Manga et al., 2012). There is no evidence for fluid flow affecting temperature. The linear temperature gradient also requires that mass movement occurred >10^4 y ago so that the temperature disturbance from emplacement has decayed (Harris et al., 2011).

Paleomagnetism

Cores 340-U1400A-1H through 9H, 340-U1400B-1H through 12H, and 340-U1400C-2H through 10H were recovered using the APC and nonmagnetic core barrels. All other APC cores were recovered using standard steel core barrels. The FlexIt core orientation tool was used with Hole U1400C APC cores recovered with nonmagnetic barrels; thus, between 15 and 95 mbsf in Hole U1400C declination can be corrected to true north. In Holes U1400A and U1400B, declination was guided by the discrete inclination (see **"Paleomagnetism"** in the "Methods" chapter [Expedition 340 Scientists, 2013a]). Expected inclination for the site is 27.4° during normal polarity and –27.4° during reversed polarity, assuming a geocentric axial dipole (GAD) model. The declination of Site U1400 from true north is approximately –15°. The archive halves of cores from Holes U1400A, U1400B, and U1400C were measured on the three-axis superconducting rock magnetometer (SRM) at 2.5 cm intervals. Natural remanent magnetization (NRM) was measured before (NRM_0) and after stepwise alternating field demagnetization at 20 mT (NRM_{20}). Sixty discrete samples were collected from the center of the working half of the core for to compare to the SRM data (see **"Paleomagnetism"** in the "Methods" chapter [Expedition 340 Scientists, 2013a]).

Sediment recovered from Site U1400 is dominated by hemipelagic sediment below a cap of coarse volcanic sand, 25–50 m thick. The hemipelagic sediment is deformed and physically inclined in both positive and negative directions varying between 20° and 80° (see **"Lithostratigraphy"**). This deformation has implications for interpretation of these data within the context of geomagnetic field behavior for Site U1400.

Results

NRM_0 (red) and NRM_{20} (blue) intensities are shown for Holes U1400A, U1400B, and U1400C in Figures **F12, F13,** and **F14.** NRM_0 intensity is high at ~1 m/A, with little difference in intensity between the overlying sand cap and the hemipelagic sediment below. The greatest downcore variation in these measurements occurs when sediment recovery changes from using nonmagnetic to steel barrels. When standard steel barrels are used to recover cores, there is an increase in sediment intensity that is not removed by demagnetization in a field of 20 mT and a persistent offset occurs between the inclination of the discrete samples and the SRM data. This is not replicated in

the magnetic susceptibility data (see **"Physical properties"**). Interpreted as a magnetic overprint by the drill string, this is a persistent feature of Expedition 340 cores recovered with steel barrels.

Hole U1400A consists almost exclusively of massive turbiditic and volcanic sand (see **"Lithostratigraphy"**) with few to no hemipelagic layers (Fig. **F12**); thus, paleomagnetic interpretations are restricted to Site U1400 to Holes U1400B and U1400C. Flexit tool–oriented declination data are available between 38.8 and 84.8 mbsf in Hole U1400C. Above this depth and to 191.1 mbsf, declination is arbitrarily rotated to a mean of 130° to match the Flexit tool–oriented declination, making for easier comparison. Rifling of the core barrel is evident by scattered declination values in all cores recovered with the XCB; thus, inclination is the only indicator of polarity below 191.1 mbsf in Hole U1400C. For Hole U1400B, declination has no true north reference and is rotated to a mean of zero and thus only be used to track relative direction within core variation (see **"Paleomagnetism"** in the "Methods" chapter [Expedition 340 Scientists, 2013a]).

Apart from two periods of negative inclination between ~28 and 38 mbsf in both holes, the zone of inclined bedding above ~385 mbsf generally shows positive inclination, as shown by both SRM and discrete data sets. SRM inclination data from nonmagnetic barrel–retrieved cores and inclination data from the majority of the discrete samples cluster, but show significant scatter, around the GAD inclination for the site. The recording of GAD-like values is surprising, considering the visible degree of deformation in the bedding. When FlexIt tool–oriented declination is available, values average ~130° during periods of positive inclination when the expected declination for the site using FlexIt-corrected data during normal polarity should be approximately –15°. Significant declination rotation also occurs within single APC cores with no associated inclination change, suggesting the magnetic directions are acting independently of each other at the site. This behavior is not characteristic of geomagnetic field behavior and is probably related to the contorted and deformed bedding at the site. That inclination values are similar to GAD-like inclination may be coincidental, but further interpretation is required to understand the processes controlling the magnetic directions at Site U1400.

Given the visible and inconsistent degree of deformation in the angle of bedding, the inclination and declination polarity disagreements in Hole U1400C, and the high degree of scatter in both the inclination and declination data sets of Holes U1400B and U1400C, we cannot interpret data from the deformed zone of Site U1400 to represent the behavior of the geomagnetic field. Although the data set does not likely maintain a geomagnetic signal, the data are of high quality and may contain information about the degree of deformation, especially if it can be determined that the sediment was initially deposited with reference to the geomagnetic field and then subsequently deformed in situ. The declination and inclination values we see in Holes U1400B and U1400C may indicate rotation associated with slumping and sediment deformation downslope but without overturning of the beds. This, however, is beyond the scope of these shipboard measurements, and further detailed investigations are required.

390 mbsf marks the lower contact of the deformed unit and hemipelagic sediments lie flatter (see **"Lithostratigraphy"**). Between 390 and 400 mbsf in Hole U1400C, both SRM and discrete samples show GAD-like negative inclination before returning to GAD-like positive inclination. Without coeval declination changes to confirm this transition, we cannot be certain that it represents geomagnetic field behavior. However, it would suggest that sediment in this normally bedded and less deformed unit was deposited during reversed polarity and is therefore at least 780 k.y. old using the geomagnetic polarity timescale (GPTS) of Cande and Kent (1995). This age would be consistent with biostratigraphic ages that suggest the age of the base of Hole U1400C sediment is Pliocene in age (see **"Paleontology and biostratigraphy"**).

References

Boudon, G., Le Friant, A., Komorowski, J.-C., Deplus, C., and Semet, M.P., 2007. Volcano flank instability in the Lesser Antilles arc: diversity of scale, processes, and temporal recurrence. *J. Geophys. Res., [Solid Earth],* 112:B08205. **doi:10.1029/2006JB004674**

Boudon, G., Le Friant, A., Villemant, B., and Viodé, J.-P., 2005. Martinique. *In* Lindsay, J.M., Robertson, R.E.A., Shepherd, J.B., and Ali, S. (Eds.), *Volcanic Hazard Atlas of the Lesser Antilles:* Trinidad and Tobago, West Indies (Seismic Research Unit, Univ. West Indies), 65–102.

Boudon, G., Semet, M.P., and Vincent, P.M., 1992. Major flank collapse at Pitons du Carbet Volcano, Martinique: one of the largest similar structures in the Lesser Antilles arc. *Proc. Int. Geol. Congr., 29th,* 505. (Abstract)

Cande, S.C., and Kent, D.V., 1995. Revised calibration of the geomagnetic polarity timescale for the Late Cretaceous and Cenozoic. *J. Geophys. Res., [Solid Earth],* 100(B4):6093–6095. **doi:10.1029/94JB03098**

Expedition 340 Scientists, 2013a. Methods. *In* Le Friant, A., Ishizuka, O., Stroncik, N.A., and the Expedition 340 Scientists, *Proc. IODP,* 340: Tokyo (Integrated Ocean Drilling Program Management International, Inc.). **doi:10.2204/iodp.proc.340.102.2013**

Expedition 340 Scientists, 2013b. Site U1394. *In* Le Friant, A., Ishizuka, O., Stroncik, N.A., and the Expedition 340

Scientists, *Proc. IODP,* 340: Tokyo (Integrated Ocean Drilling Program Management International, Inc.). **doi:10.2204/iodp.proc.340.104.2013**

Expedition 340 Scientists, 2013c. Site U1398. *In* Le Friant, A., Ishizuka, O., Stroncik, N.A., and the Expedition 340 Scientists, *Proc. IODP,* 340: Tokyo (Integrated Ocean Drilling Program Management International, Inc.). **doi:10.2204/iodp.proc.340.108.2013**

Harris, R.N., Schmidt-Schierhorn, F., and Spinelli, G., 2011. Heat flow along the NanTroSEIZE transect: results from IODP Expeditions 315 and 316 offshore the Kii Peninsula, Japan. *Geochem., Geophys., Geosyst.,* 12:Q0AD16. **doi:10.1029/2011GC003593**

Hayward, B.W., Kawagata, S., Grenfell, H.R., Droxler, A.W., and Shearer, M., 2006. Mid-Pleistocene extinction of bathyal benthic foraminifera in the Caribbean Sea. *Micropaleontology,* 52(3):245–265. **doi:10.2113/gsmicropal.52.3.245**

Kameo, K., and Bralower, T.J., 2000. Neogene calcareous nannofossil biostratigraphy of Sites 998, 999, and 1000, Caribbean Sea. *In* Leckie, R.M., Sigurdsson, H., Acton, G.D., and Draper, G. (Eds.), *Proc. ODP, Sci. Results,* 165: College Station, TX (Ocean Drilling Program), 3–17. **doi:10.2973/odp.proc.sr.165.012.2000**

Le Friant, A., Boudon, G., Deplus C., and Villemant B., 2003. Large-scale flank collapse events during the activity of Montagne Pelée, Martinique, Lesser Antilles. *J. Geophys. Res., [Solid Earth],* 108(B1):2055. **doi:10.1029/2001JB001624**

Manga, M., Hornbach, M.J., Le Friant, A., Ishizuka, O., Stroncik, N., Adachi, T., Aljahdali, M., Boudon, G., Breitkreuz, C., Fraass, A., Fujinawa, A., Hatfield, R., Jutzeler, M., Kataoka, K., Lafuerza, S., Maeno, F., Martinez-Colon, M., McCanta, M., Morgan, S., Palmer, M.R., Saito, T., Slagle, A., Stinton, A.J., Subramanyam, K.S.V., Tamura, Y., Talling, P.J., Villemant, B., Wall-Palmer, D., and Wang, F., 2012. Heat flow in the Lesser Antilles island arc and adjacent backarc Grenada Basin. *Geochem., Geophys., Geosyst.,* 13:Q08007. **doi:10.1029/2012GC004260**

Okada, H., and Bukry, D., 1980. Supplementary modification and introduction of code numbers to the low-latitude coccolith biostratigraphic zonation (Bukry, 1973; 1975). *Mar. Micropaleontol.,* 5:321–325. **doi:10.1016/0377-8398(80)90016-X**

Samper, A., Quidelleur, X., Lahitte, P., and Mollex, D., 2007. Timing of effusive volcanism and collapse events within an oceanic arc island: Basse-Terre, Guadeloupe archipelago (Lesser Antilles arc). *Earth Planet. Sci. Lett.,* 258(1–2):175–191. **doi:10.1016/j.epsl.2007.03.030**

Publication: 17 August 2013
MS 340-110

Figure F1. Site U1400 maps. **A.** Shaded image of topography-bathymetry, chaotic deposits (interpreted as debris avalanche deposits), and drill sites, Expedition 340. DAD = debris avalanche deposit. (Continued on next page.)

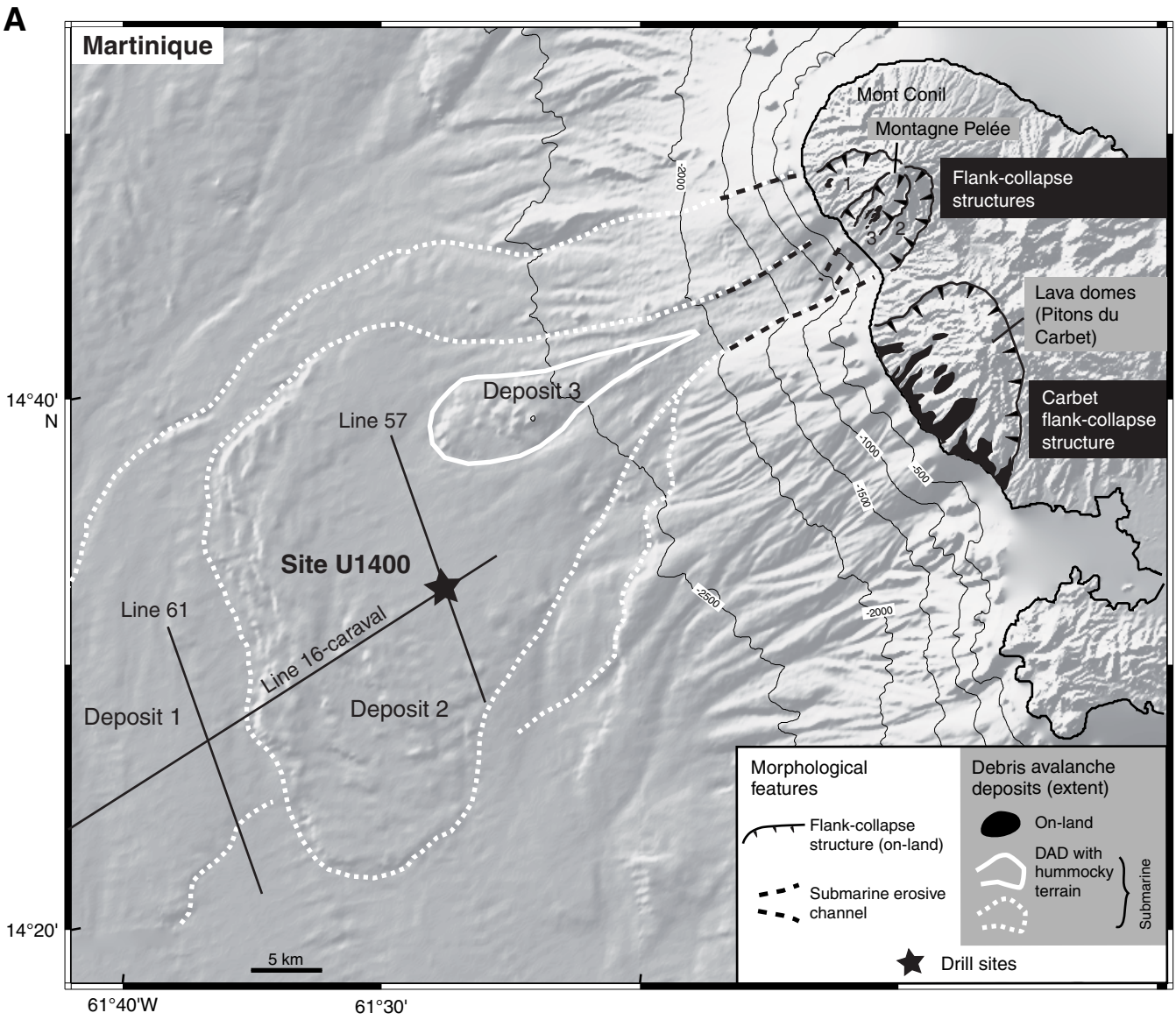

Figure F1 (continued). B. Location of seismic reflection lines across the Site U1400. CDP = common depth point.

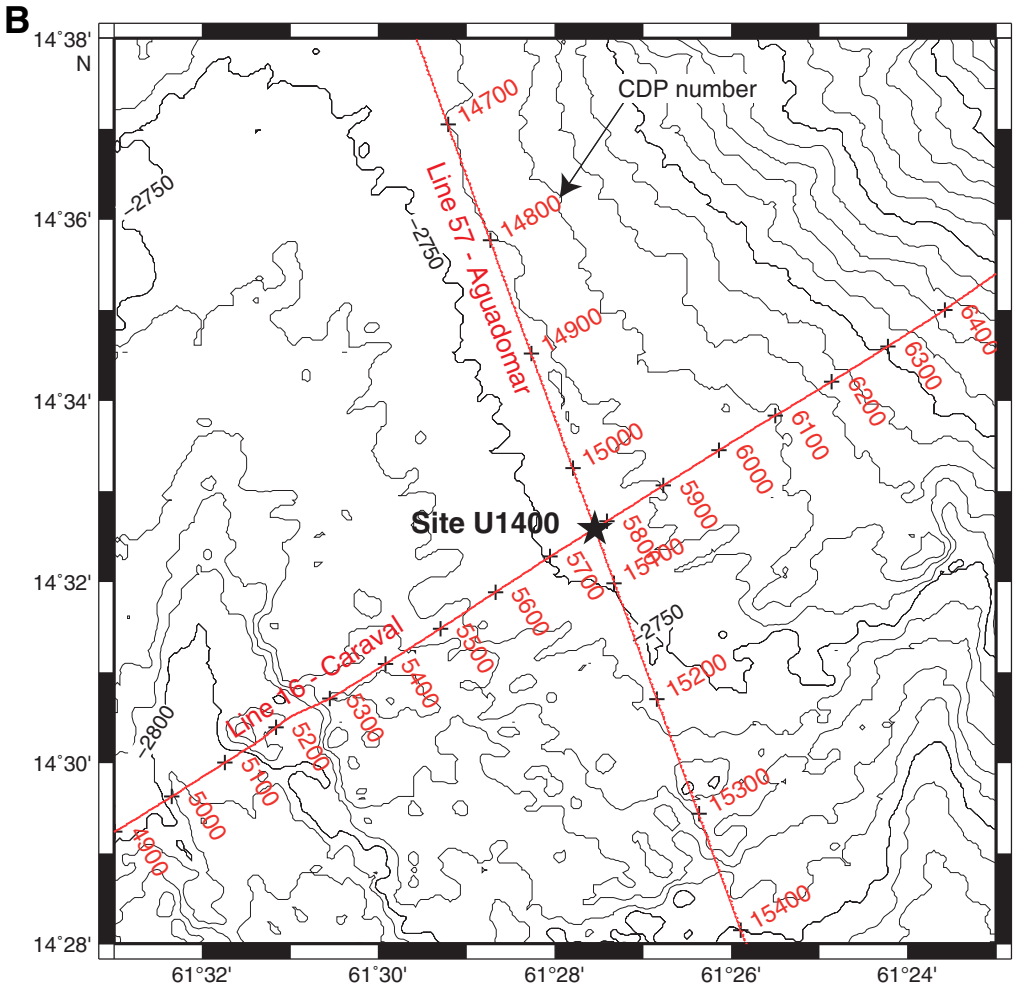

Figure F2. Plot showing the location of lithostratigraphic Units A–G in Holes U1400A–U1400C. Unit A is not observed in Hole C because the first 15 mbsf were drilled without recovery.

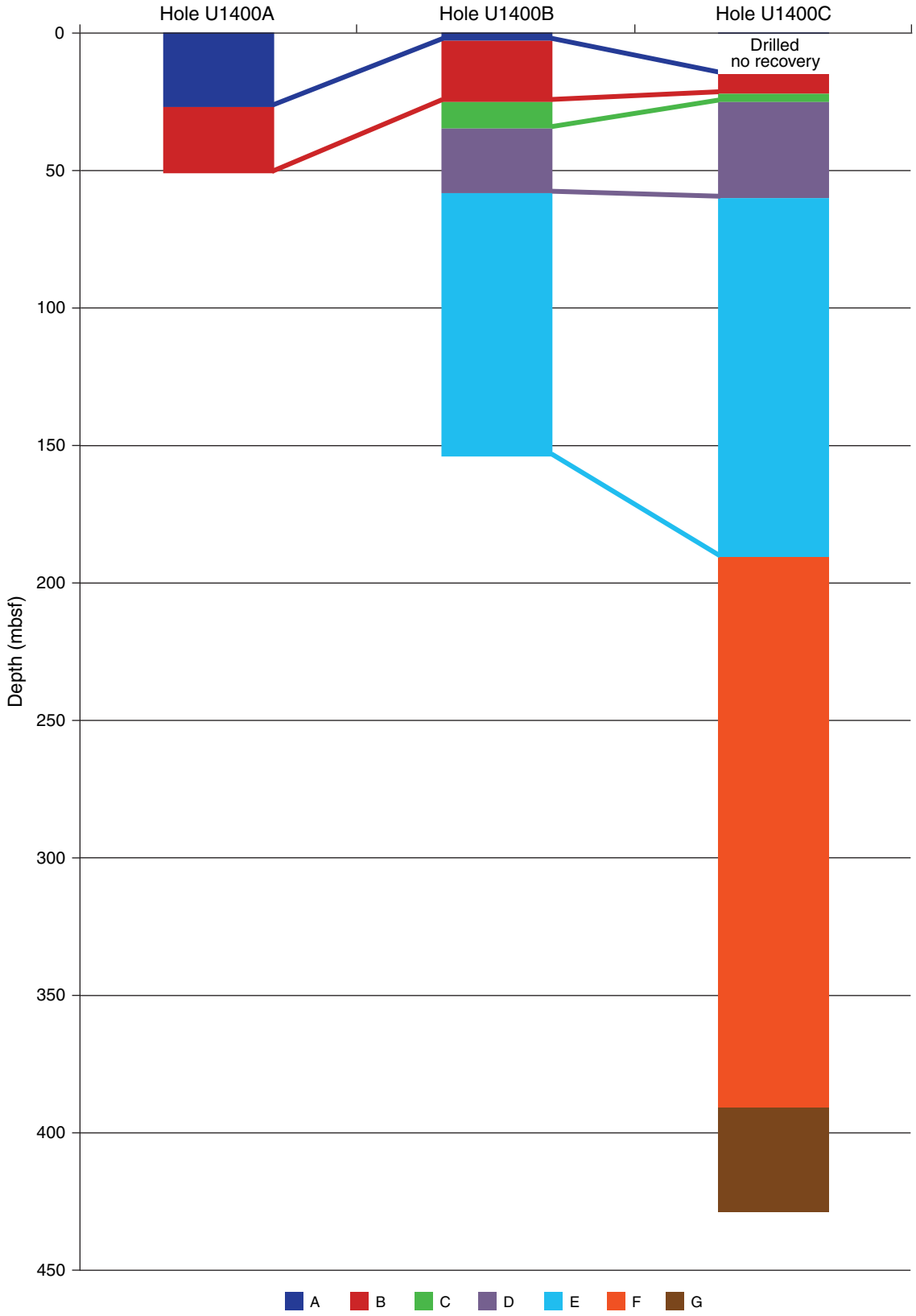

Figure F3. Integrated nannofossil and planktonic foraminiferal biozonation, Site U1400.

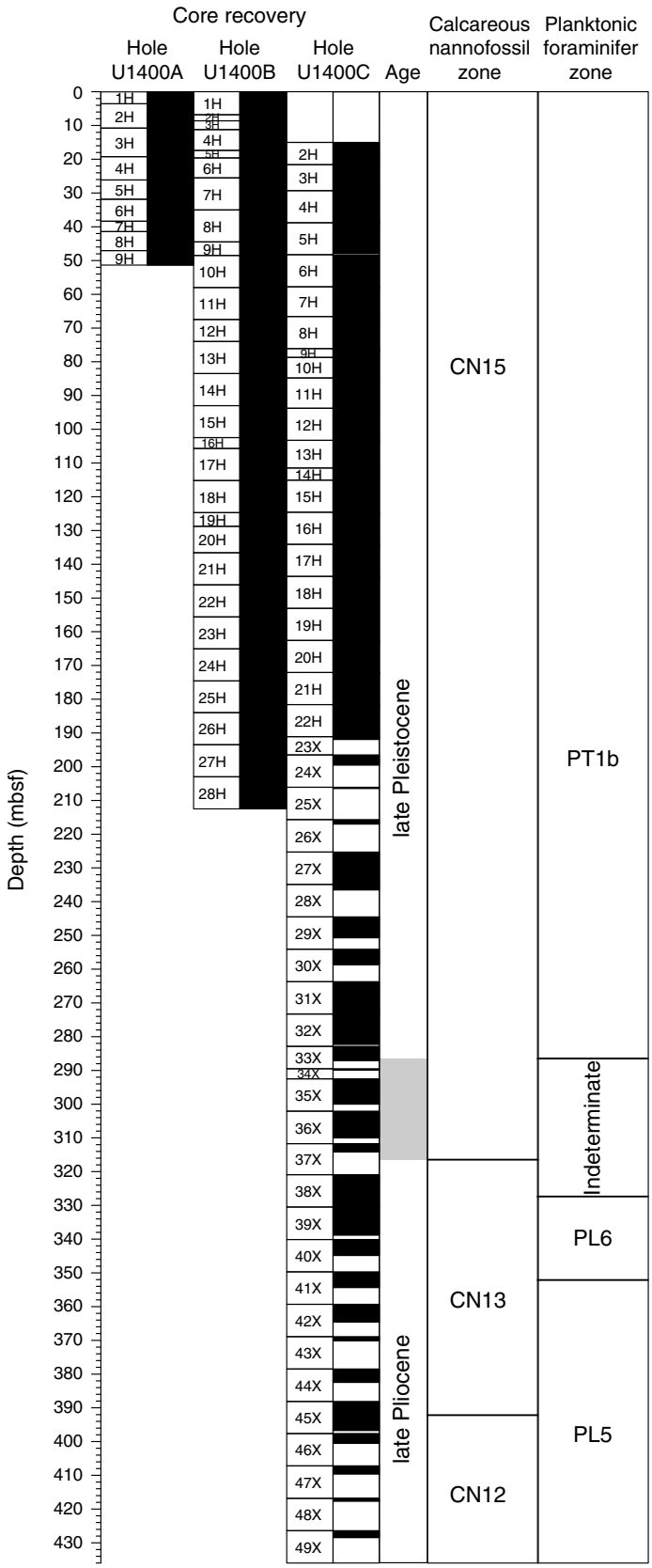

Figure F4. Summary of planktonic foraminiferal biozonation, Site U1400. Species *Globigerinella calida*, *Globorotalia miocenica*, *Globorotalia exilis*, and *Globigerinoides extremus* are believed to represent the true age of the deposits. *Globorotalia flexuosa* may represent a true age, but this is not conclusive, given the few samples in which it is present. *Globorotalia tosaensis* and *Globorotalia cibaoensis* are likely reworked from older material. The bottom of *G. tosaensis* in Hole U1400C is unclear, indicated by the blue question marks. Black question marks denote the unclear relationship below the cored material. Correlations between sites are based on the species present and their age ranges, not lithology.

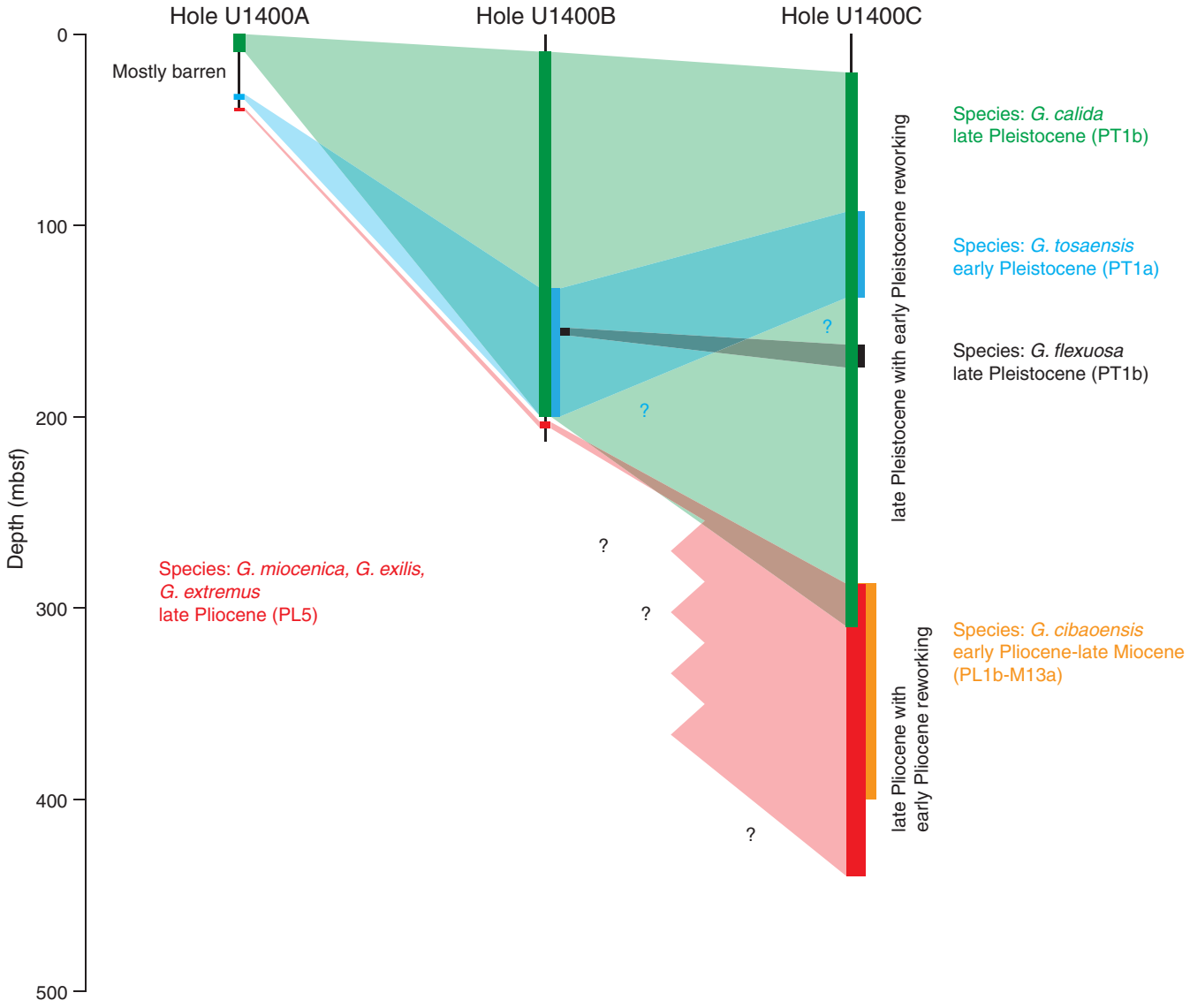

Figure F5. XRD patterns of selected samples from Hole U1400B. **A.** Sample 340-U1400B-3H-2, 63–64 cm. (Continued on next page.)

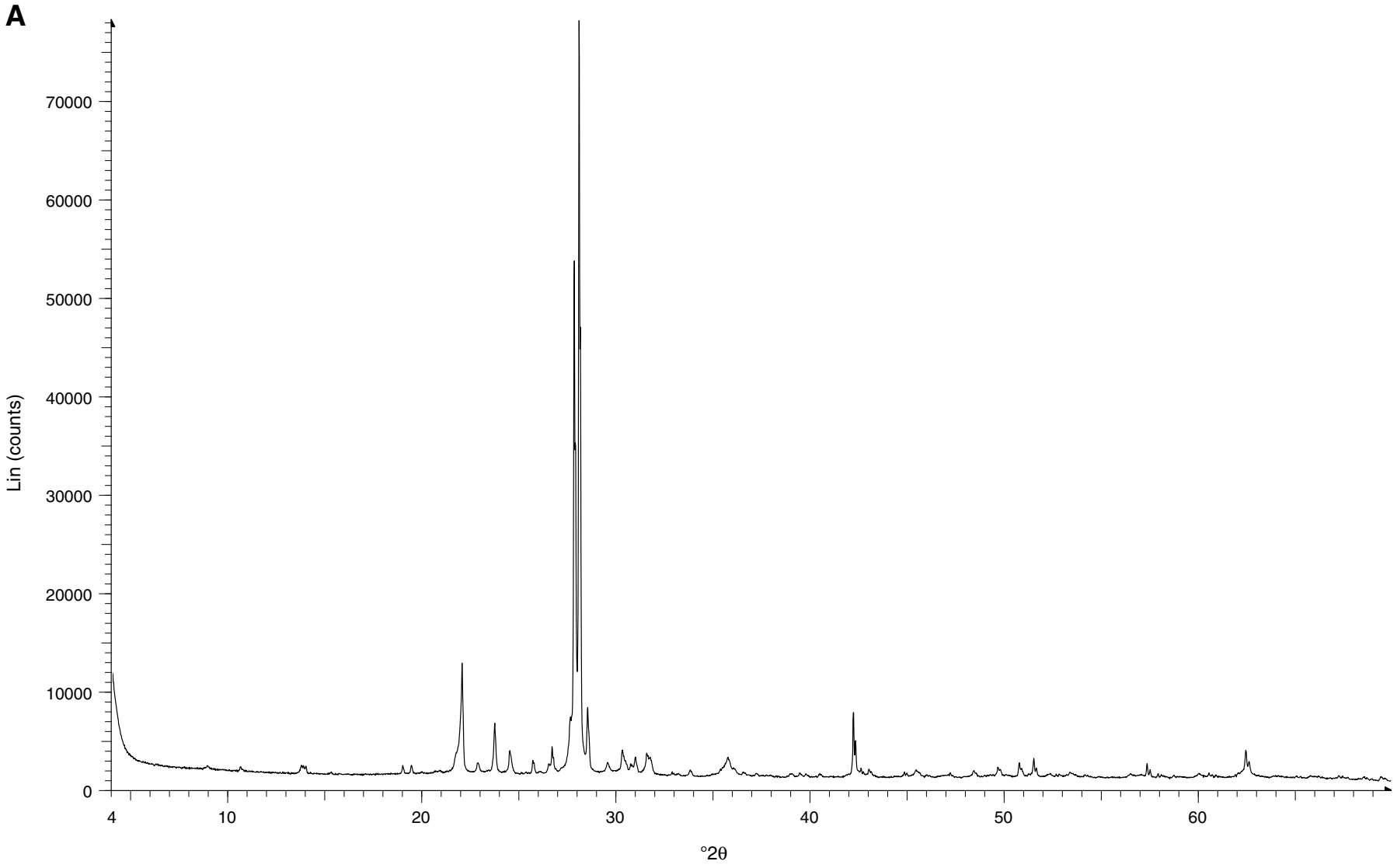

Figure F5 (continued). B. Sample 340-U1400B-7H-3, 51–52 cm.

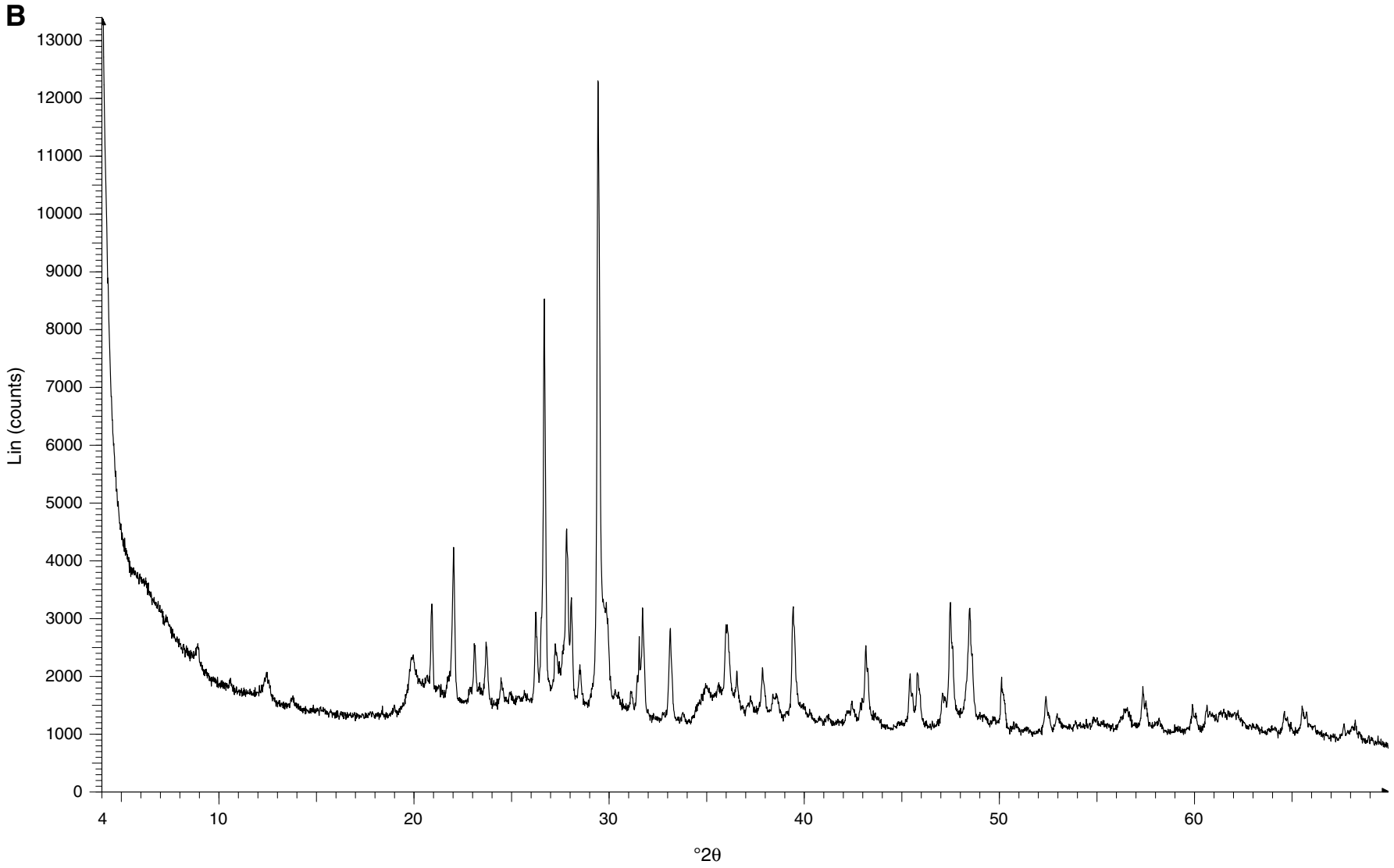

Figure F6. Solid-phase geochemical depth profiles, Site U1400. **A.** $CaCO_3$. **B.** Organic carbon.

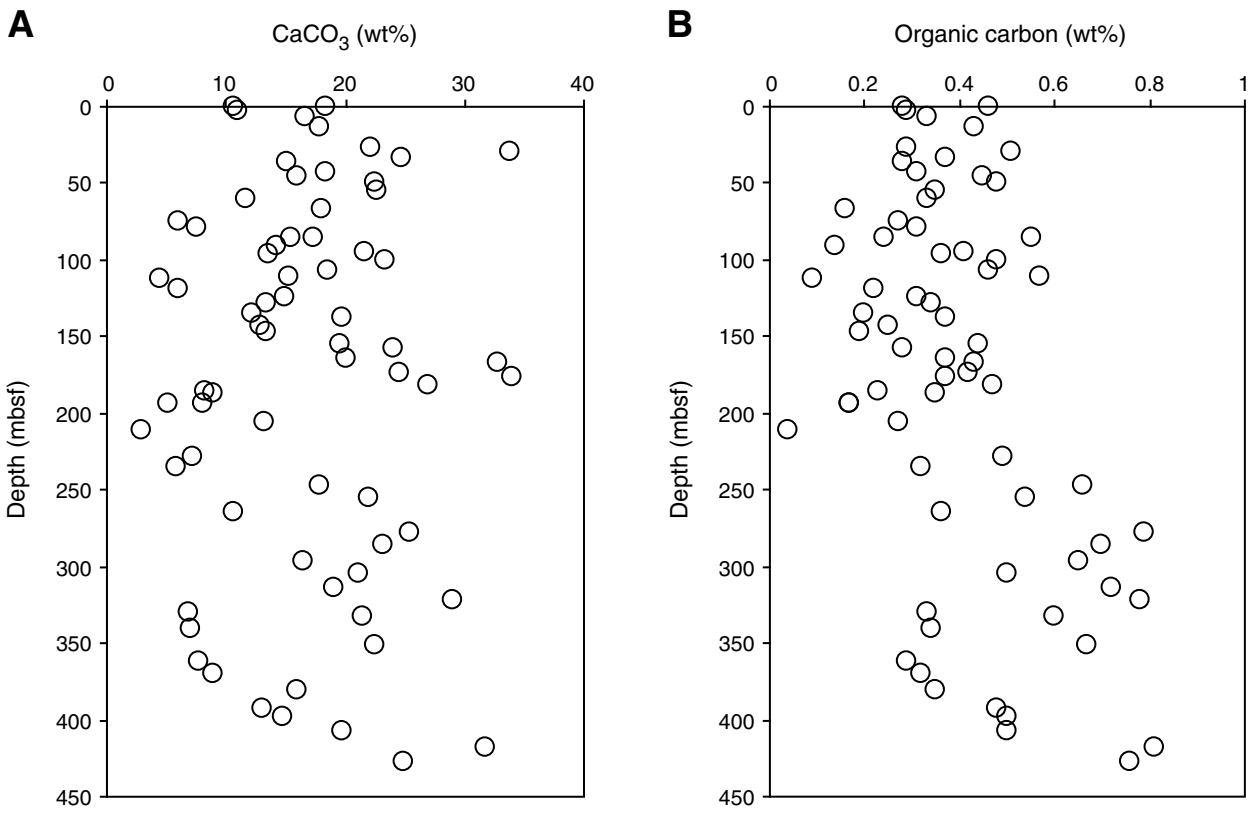

Figure F7. Pore water geochemical depth profiles, Site U1400. **A.** Alkalinity. **B.** NH_4^+. **C.** Ca. **D.** Mg. **E.** Cl. **F.** ΣS.

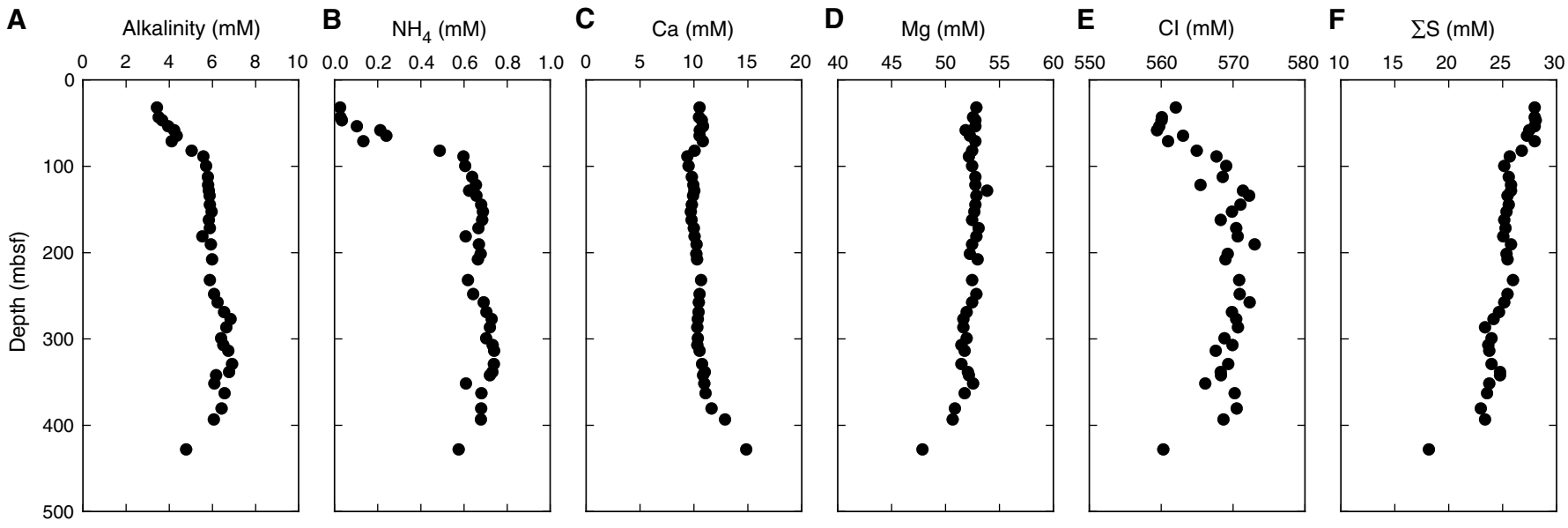

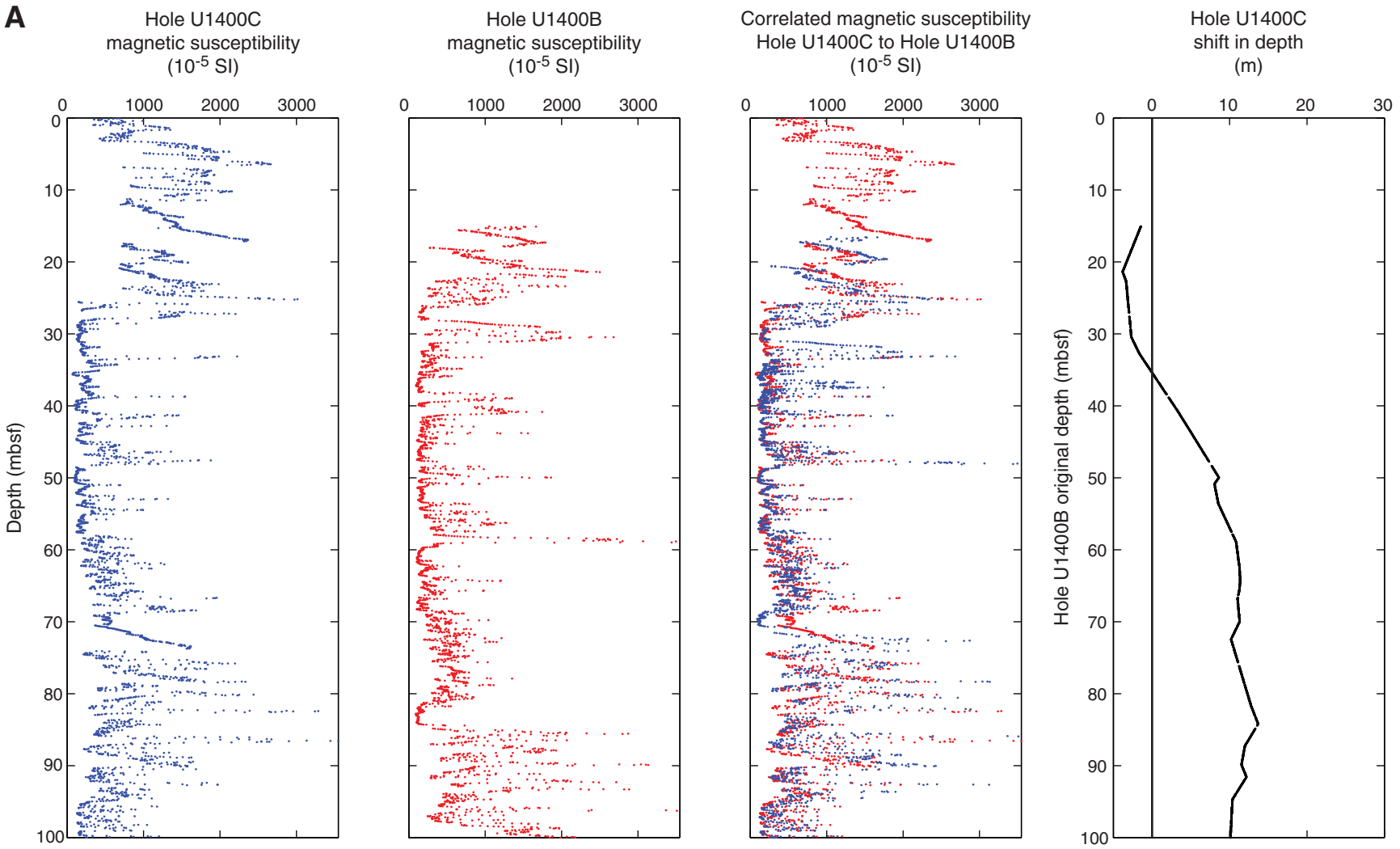

Figure F8. Magnetic susceptibility correlation, Hole U1400C (blue) to Hole U1400B (red). Magnetic susceptibility was measured on the Whole-Round Multisensor Logger (WRMSL). Negative values in the last column indicate a downhole shift. **A.** 0–100 mbsf. (Continued on next page.)

Figure F8 (continued). B. 100–200 mbsf.

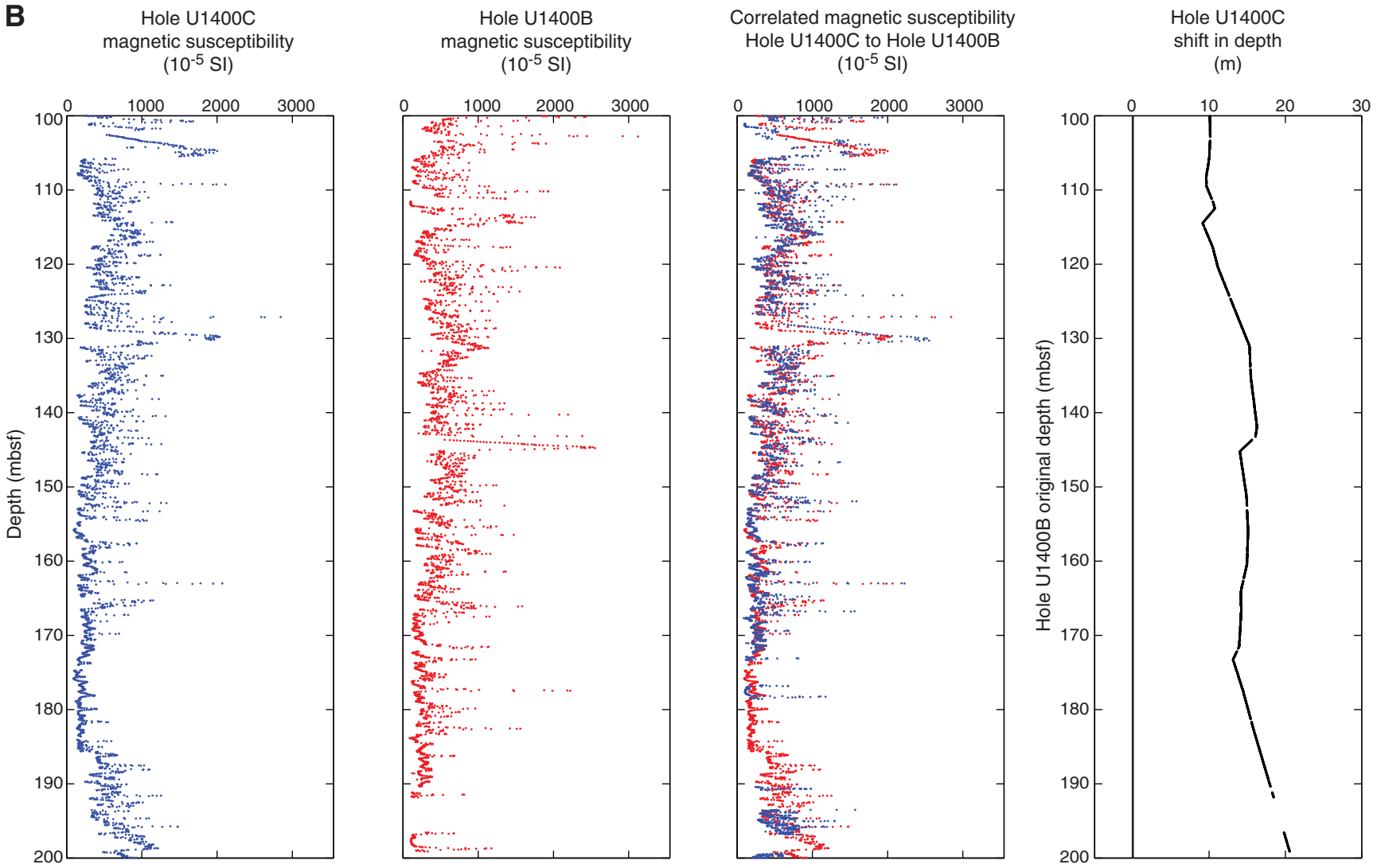

Figure F9. Physical properties, Holes U1400A (red), U1400B (green), and U1400C (blue), 0–55 mbsf. AVS = automated vane shear. Small points indicate measurements on whole cores using the Whole-Round Multisensor Logger (WRMSL) or Natural Gamma Radiation Logger (NGRL). Larger circles indicate spot measurements obtained from samples of the split working half of the core.

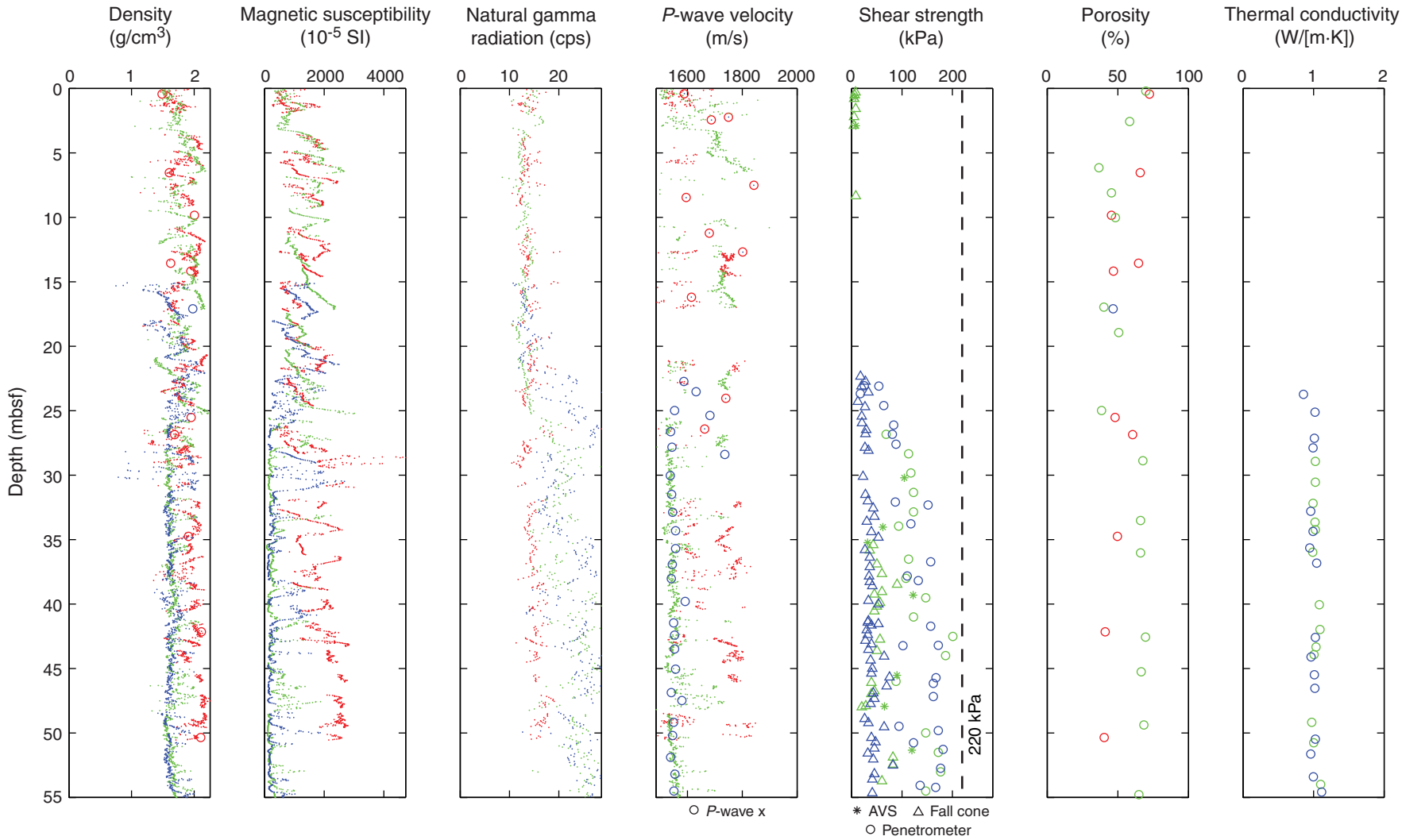

Figure F10. Physical properties, Holes U1400A (red), U1400B (green), and U1400C (blue), 0–437 mbsf. AVS = automated vane shear. Small points indicate measurements on whole cores using the Whole-Round Multisensor Logger (WRMSL) or Natural Gamma Radiation Logger (NGRL). Larger circles indicate spot measurements obtained from samples of the split working half of the core.

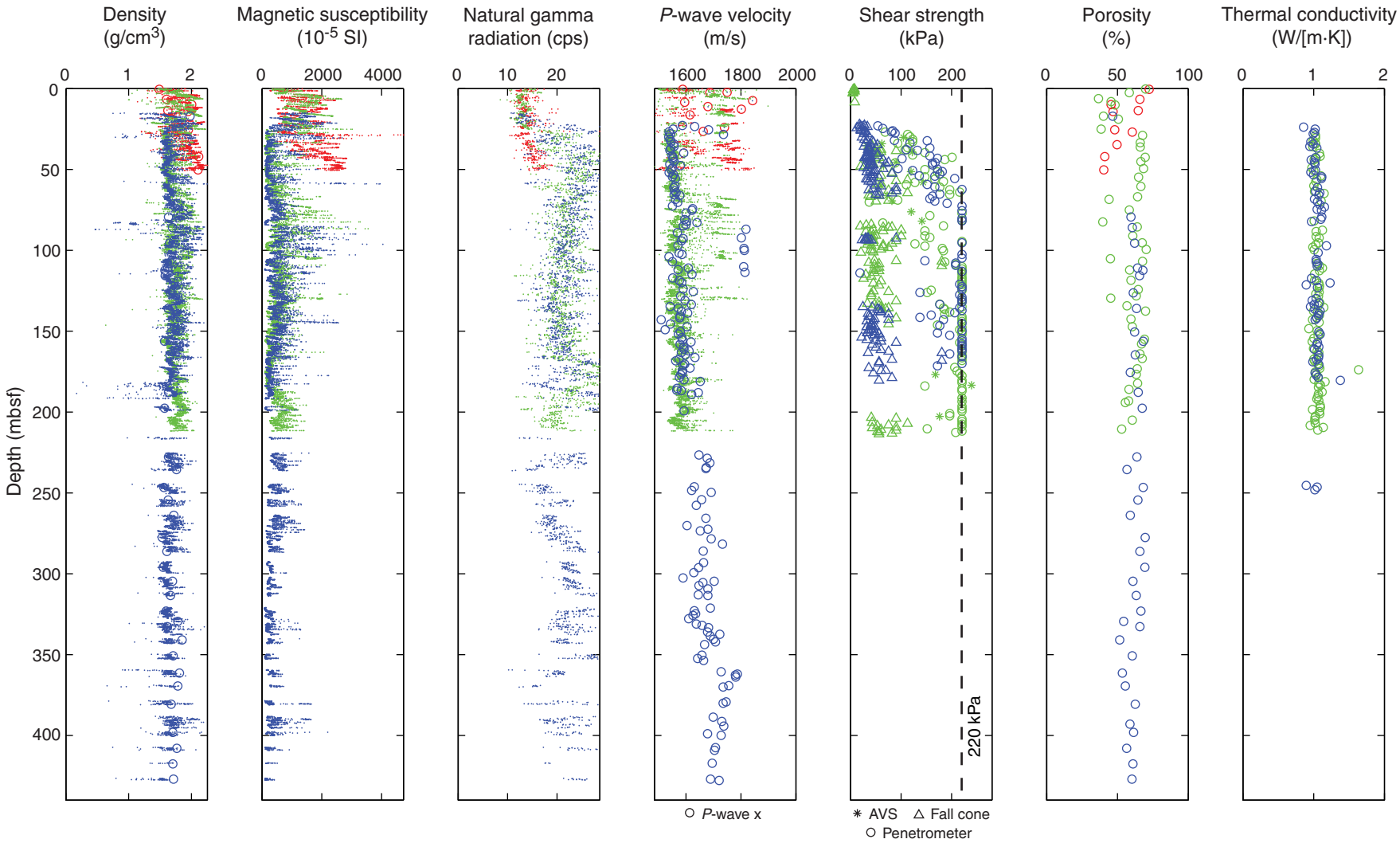

Figure F11. Temperature as a function of depth, Hole U1400C. Straight line is a best fit to the measurements.

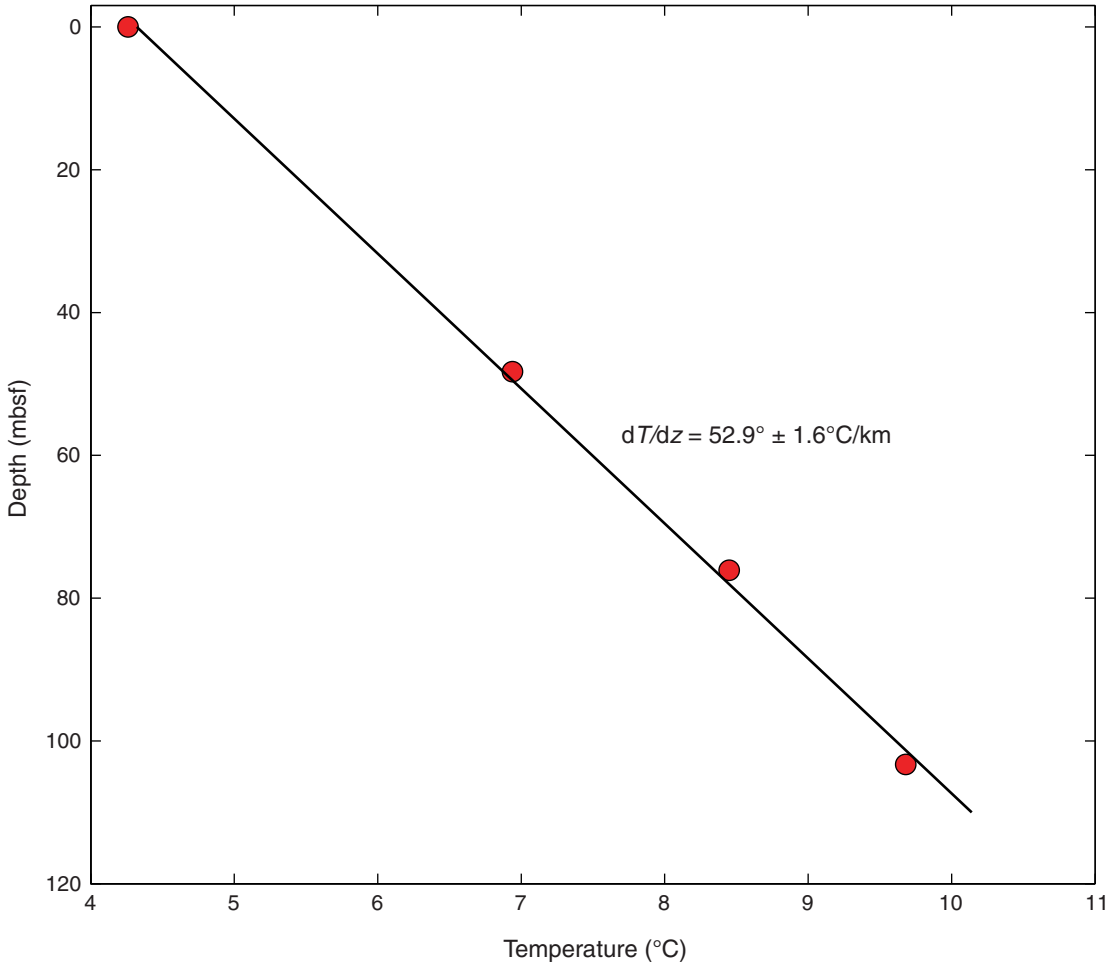

Figure F12. Plots of intensity of NRM_0 (red) and NRM_{20} (blue) and inclination and declination after 20 mT demagnetization, Hole U1400A. For inclination data, gray points are all measurements made and red data are measurements made on hemipelagic sediment shown against a geocentric axial dipole (GAD) inclination of 27.4°. For declination data, gray points are unoriented declinations and red points are FlexIt tool–corrected data on hemipelagic sediment.

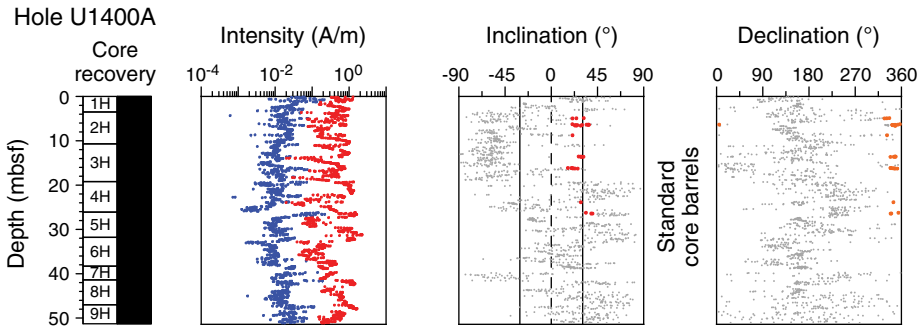

Figure F13. Plots of intensity of NRM_0 (red) and NRM_{20} (blue) and inclination and declination after 20 mT demagnetization, Hole U1400B. For inclination data, gray points are all measurements made and red data are measurements made on hemipelagic sediment shown against a geocentric axial dipole (GAD) inclination of 27.4°. For declination data, gray points are unoriented declinations and orange points are SRM and discrete inclination guided data on hemipelagic sediment. Black squares are discrete declination and inclination measurements.

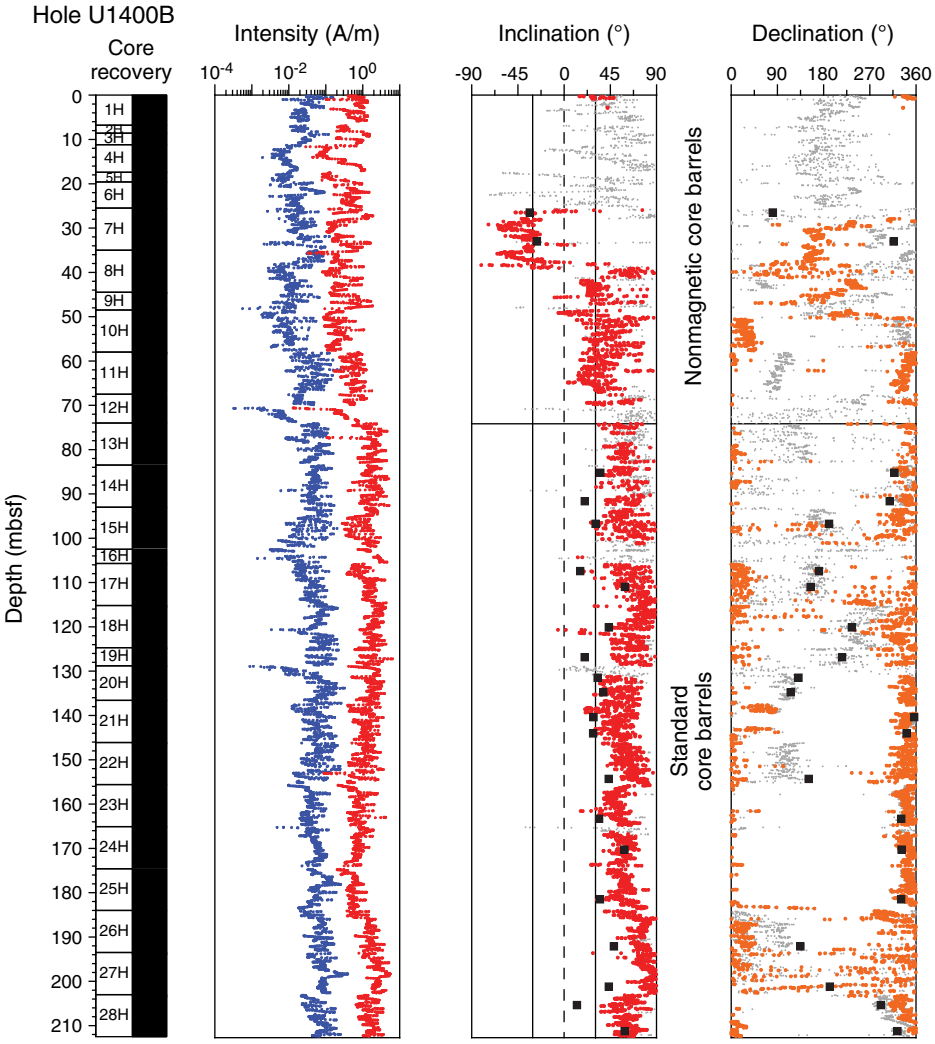

Figure F14. Plots of intensity of NRM_0 (red) and NRM_{20} (blue) and inclination and declination after 20 mT demagnetization, Hole U1400C. For inclination data, gray points are all measurements made and red data are measurements made on hemipelagic sediment shown against a geocentric axial dipole (GAD) inclination of 27.4°. For declination data, gray points are unoriented declinations and red points are FlexIt tool–corrected data on hemipelagic sediment. Orange points are data on hemipelagic sediment rotated to a mean of 130°. Black squares are discrete declination and inclination measurements.

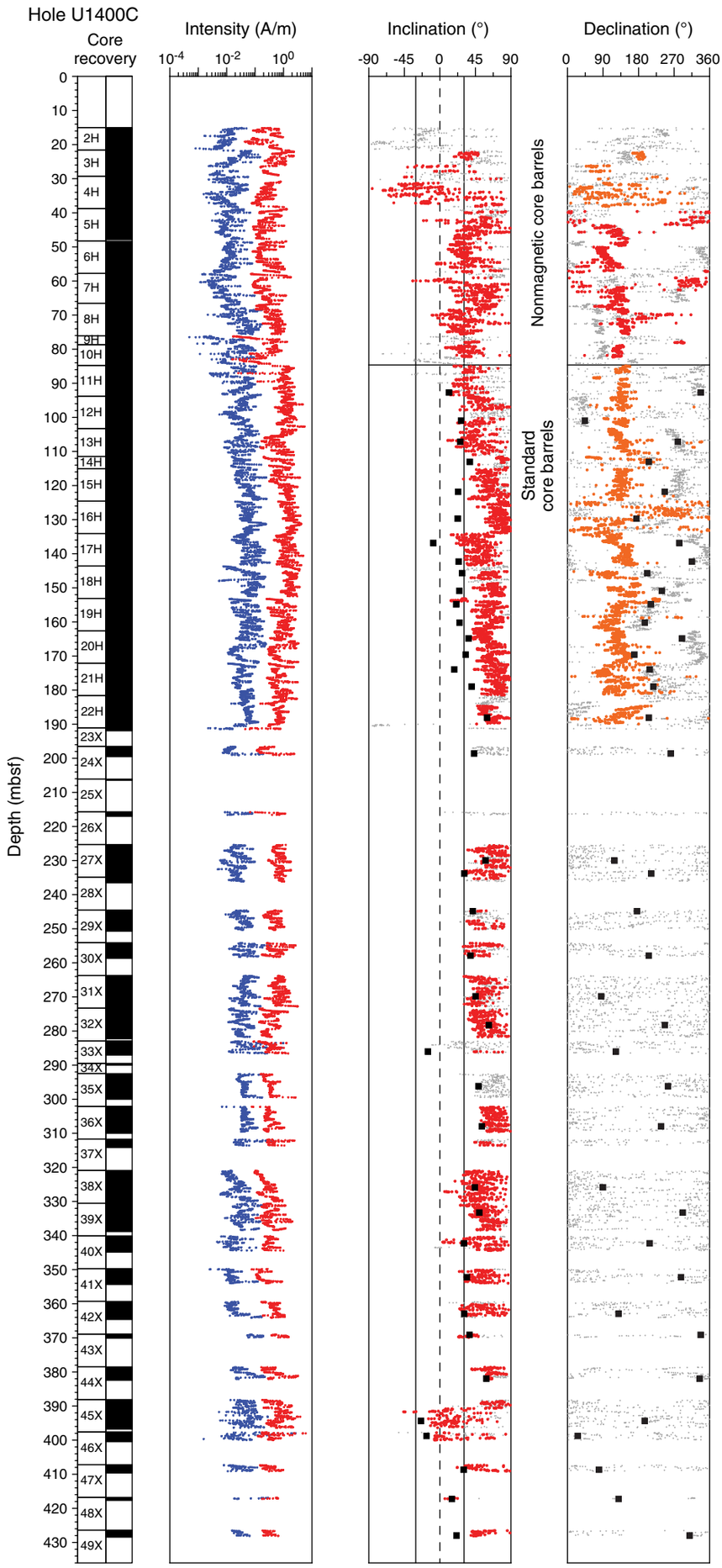

Table T1. Coring summary, Site U1400. (Continued on next page.)

Hole:	U1400A
Latitude:	14°32.5831′N
Longitude:	61°27.5492′W
Water depth (m):	2744.35
Date started (UTC*):	1230 h 4 April 2012
Date finished (UTC*):	1045 h 5 April 2012
Time on hole (days):	0.9
Seafloor depth DRF (m):	2756
Penetration DSF (m):	51.3
Cored interval (m):	51.3
Recovered length (m):	51.80
Recovery (%):	101
Total cores (no.):	9
Hole:	U1400B
Latitude:	14°32.2023′N
Longitude:	61°27.4065′W
Water depth (m):	2743.05
Date started (UTC*):	1045 h 5 April 2012
Date finished (UTC*):	0630 h 7 April 2012
Time on hole (days):	1.8
Seafloor depth DRF (m):	2754.7
Penetration DSF (m):	212.5
Cored interval (m):	212.5
Recovered length (m):	215.19
Recovery (%):	101
Total cores (no.):	28
Hole:	U1400C
Latitude:	14°32.1935′N
Longitude:	61°27.4028′W
Water depth (m):	2743.0
Date started (UTC*):	0630 h 7 April 2012
Date finished (UTC*):	0330 h 13 April 2012
Time on hole (days):	5.9
Seafloor depth DRF (m):	2754.7
Penetration DSF (m):	436.0
Cored interval (m):	421.0
Recovered length (m):	304.49
Recovery (%):	72
Drilled interval (m):	15
Drilled interval (no.):	1
Total cores (no.):	48

Core	Top depth drilled DSF (m)	Bottom depth drilled DSF (m)	Advanced (m)	Recovered length (m)	Curated length (m)	Top depth cored CSF (m)	Bottom depth recovered CSF (m)	Recovery (%)	Time on deck (UTC*)
340-U1400A-									
1H	0.0	3.5	3.5	3.59	3.59	0.0	3.59	103	4/5/12 04:45
2H	3.5	10.7	7.2	7.25	7.25	3.5	10.75	101	4/5/12 07:30
3H	10.7	19.2	8.5	8.54	8.54	10.7	19.24	100	4/5/12 08:20
4H	19.2	26.1	6.9	6.97	6.97	19.2	26.17	101	4/5/12 09:20
5H	26.1	31.8	5.7	5.77	5.77	26.1	31.87	101	4/5/12 10:20
6H	31.8	38.3	6.5	6.50	6.50	31.8	38.30	100	4/5/12 11:45
7H	38.3	41.4	3.1	3.14	3.14	38.3	41.44	101	4/5/12 12:45
8H	41.4	47.0	5.6	5.65	5.65	41.4	47.05	101	4/5/12 13:45
9H	47.0	51.3	4.3	4.39	4.39	47.0	51.39	102	4/5/12 15:25
340-U1400B-									
1H	0.0	6.8	6.8	6.82	6.82	0.0	6.82	100	4/5/12 20:20
2H	6.8	8.6	1.8	1.83	1.83	6.8	8.63	102	4/5/12 21:25
3H	8.6	11.2	2.6	2.60	2.60	8.6	11.20	100	4/5/12 22:20
4H	11.2	17.4	6.2	6.29	6.29	11.2	17.49	101	4/5/12 23:10
5H	17.4	19.6	2.2	2.27	2.27	17.4	19.67	103	4/6/12 00:05
6H	19.6	25.5	5.9	5.92	5.92	19.6	25.52	100	4/6/12 00:50
7H	25.5	35.0	9.5	9.44	9.44	25.5	34.94	99	4/6/12 01:40
8H	35.0	44.5	9.5	9.80	9.80	35.0	44.80	103	4/6/12 02:50
9H	44.5	48.5	4.0	4.01	4.01	44.5	48.51	100	4/6/12 03:25
10H	48.5	58.0	9.5	9.90	9.90	48.5	58.40	104	4/6/12 04:20
11H	58.0	67.5	9.5	9.31	9.31	58.0	67.31	98	4/6/12 05:20
12H	67.5	74.0	6.5	6.50	6.50	67.5	74.00	100	4/6/12 05:55
13H	74.0	83.5	9.5	9.23	9.23	74.0	83.23	97	4/6/12 07:20
14H	83.5	93.0	9.5	9.57	9.57	83.5	93.07	101	4/6/12 08:05

Table T1 (continued).

Core	Top depth drilled DSF (m)	Bottom depth drilled DSF (m)	Advanced (m)	Recovered length (m)	Curated length (m)	Top depth cored CSF (m)	Bottom depth recovered CSF (m)	Recovery (%)	Time on deck (UTC*)
15H	93.0	102.5	9.5	9.16	9.16	93.0	102.16	96	4/6/12 08:50
16H	102.5	105.7	3.2	3.23	3.23	102.5	105.73	101	4/6/12 10:05
17H	105.7	115.2	9.5	9.86	9.86	105.7	115.56	104	4/6/12 11:50
18H	115.2	124.7	9.5	9.79	9.79	115.2	124.99	103	4/6/12 13:15
19H	124.7	128.8	4.1	4.18	4.18	124.7	128.88	102	4/6/12 14:15
20H	128.8	136.6	7.8	7.87	7.87	128.8	136.67	101	4/6/12 15:25
21H	136.6	146.1	9.5	9.85	9.85	136.6	146.45	104	4/6/12 16:45
22H	146.1	155.6	9.5	9.53	9.53	146.1	155.63	100	4/6/12 18:00
23H	155.6	165.1	9.5	9.63	9.63	155.6	165.23	101	4/6/12 18:40
24H	165.1	174.6	9.5	9.22	9.22	165.1	174.32	97	4/6/12 19:25
25H	174.6	184.0	9.4	9.45	9.45	174.6	184.05	101	4/6/12 20:15
26H	184.0	193.5	9.5	10.00	10.00	184.0	194.00	105	4/6/12 21:40
27H	193.5	203.0	9.5	10.03	10.03	193.5	203.53	106	4/6/12 22:35
28H	203.0	212.5	9.5	9.90	9.90	203.0	212.90	104	4/7/12 13:25
340-U1400C-									
11			*****Drilled from 0 to 15.0 mbsf*****						4/8/12 15:15
2H	15.0	21.6	6.6	6.69	6.69	15.0	21.69	101	4/8/12 16:00
3H	21.6	29.3	7.7	7.79	7.79	21.6	29.39	101	4/8/12 17:00
4H	29.3	38.8	9.5	9.77	9.77	29.3	39.07	103	4/8/12 17:50
5H	38.8	48.3	9.5	9.07	9.07	38.8	47.87	95	4/8/12 19:20
6H	48.3	57.8	9.5	9.92	9.92	48.3	58.22	104	4/8/12 20:15
7H	57.8	66.6	8.8	8.83	8.83	57.8	66.63	100	4/8/12 21:00
8H	66.6	76.1	9.5	10.06	10.06	66.6	76.66	106	4/8/12 22:25
9H	76.1	78.7	2.6	2.63	2.63	76.1	78.73	101	4/8/12 23:20
10H	78.7	84.8	6.1	6.19	6.19	78.7	84.89	101	4/9/12 00:15
11H	84.8	93.8	9.0	9.09	9.09	84.8	93.89	101	4/9/12 01:05
12H	93.8	103.3	9.5	9.76	9.76	93.8	103.56	103	4/9/12 02:40
13H	103.3	111.5	8.2	8.24	8.24	103.3	111.54	100	4/9/12 03:50
14H	111.5	115.1	3.6	3.63	3.63	111.5	115.13	101	4/9/12 04:25
15H	115.1	124.6	9.5	9.84	9.84	115.1	124.94	104	4/9/12 05:45
16H	124.6	134.1	9.5	9.81	9.81	124.6	134.41	103	4/9/12 08:00
17H	134.1	143.6	9.5	10.01	10.01	134.1	144.11	105	4/9/12 09:05
18H	143.6	153.1	9.5	9.30	9.30	143.6	152.90	98	4/9/12 09:45
19H	153.1	162.6	9.5	9.98	9.98	153.1	163.08	105	4/9/12 11:05
20H	162.6	172.1	9.5	10.00	10.00	162.6	172.60	105	4/9/12 12:10
21H	172.1	181.6	9.5	9.94	9.94	172.1	182.04	105	4/9/12 12:45
22H	181.6	191.1	9.5	9.80	9.80	181.6	191.40	103	4/9/12 13:25
23X	191.1	196.5	5.4	0.85	0.85	191.1	191.95	16	4/9/12 17:05
24X	196.5	206.1	9.6	3.05	3.05	196.5	199.55	32	4/9/12 18:30
25X	206.1	215.7	9.6	0.37	0.37	206.1	206.47	4	4/9/12 20:20
26X	215.7	225.3	9.6	1.34	1.34	215.7	217.04	14	4/9/12 21:45
27X	225.3	234.9	9.6	9.74	9.74	225.3	235.04	101	4/9/12 23:00
28X	234.9	244.5	9.6	1.62	1.62	234.9	236.52	17	4/10/12 00:20
29X	244.5	254.1	9.6	6.23	6.23	244.5	250.73	65	4/10/12 01:45
30X	254.1	263.7	9.6	4.61	4.61	254.1	258.71	48	4/10/12 03:00
31X	263.7	273.3	9.6	9.84	9.84	263.7	273.54	103	4/10/12 04:15
32X	273.3	282.9	9.6	8.99	8.99	273.3	282.29	94	4/10/12 05:35
33X	282.9	289.5	6.6	4.17	4.17	282.9	287.07	63	4/10/12 07:15
34X	289.5	292.5	3.0	0.45	0.45	289.5	289.95	15	4/10/12 08:40
35X	292.5	302.1	9.6	7.53	7.53	292.5	300.03	78	4/10/12 10:05
36X	302.1	311.7	9.6	7.91	7.91	302.1	310.01	82	4/10/12 11:30
37X	311.7	320.9	9.2	2.51	2.51	311.7	314.21	27	4/10/12 13:00
38X	320.9	330.5	9.6	9.75	9.75	320.9	330.65	102	4/10/12 14:25
39X	330.5	340.1	9.6	8.35	8.35	330.5	338.85	87	4/10/12 15:45
40X	340.1	349.7	9.6	4.76	4.76	340.1	344.86	50	4/10/12 17:15
41X	349.7	359.3	9.6	4.67	4.67	349.7	354.37	49	4/10/12 18:55
42X	359.3	368.9	9.6	5.31	5.31	359.3	364.61	55	4/10/12 21:00
43X	368.9	378.5	9.6	1.21	1.21	368.9	370.11	13	4/10/12 23:05
44X	378.5	388.1	9.6	3.96	3.96	378.5	382.46	41	4/11/12 00:35
45X	388.1	397.6	9.5	8.63	8.63	388.1	396.73	91	4/11/12 02:05
46X	397.6	407.2	9.6	2.87	2.87	397.6	400.47	30	4/11/12 03:40
47X	407.2	416.8	9.6	2.46	2.46	407.2	409.66	26	4/11/12 05:55
48X	416.8	426.4	9.6	0.89	0.89	416.8	417.69	9	4/11/12 08:20
49X	426.4	436.0	9.6	2.07	2.07	426.4	428.47	22	4/11/12 10:10
		Totals:	699.8	571.48	571.48				

* = ship local time was Universal Time Coordinated (UTC) – 4 h. DRF = drilling depth below rig floor, DSF = drilling depth below seafloor, CSF = core depth below seafloor. H = advanced piston corer, X = extended core barrel.

Table T2. Solid-phase geochemistry, Site U1400. (Continued on next page.)

Core, section	Depth (mbsf)		Carbon (wt%)				Nitrogen (wt%)
	Top	Bottom	$CaCO_3$	Inorganic	Total	Organic	
340-U1400A-							
1H-1	0.40	0.41	10.59	1.27	1.55	0.28	0.03
2H-3	6.52	6.53	16.62	1.99	2.32	0.33	0.03
3H-3	13.53	13.54	17.81	2.14	2.56	0.43	0.03
5H-1	26.88	26.89	22.19	2.66	2.95	0.29	0.02
340-U1400B-							
1H-1	0.19	0.20	18.32	2.20	2.66	0.46	0.05
1H-2	2.55	2.56	11.01	1.32	1.61	0.29	0.01
7H-3	28.85	28.86	33.88	4.06	4.57	0.51	0.03
7H-6	33.49	33.50	24.65	2.96	3.33	0.37	0.02
8H-1	36.02	36.03	15.14	1.82	2.09	0.28	0.01
8H-6	42.76	42.77	18.39	2.21	2.52	0.31	0.03
9H-1	45.23	45.24	15.96	1.91	2.36	0.45	0.03
10H-1	49.38	49.39	22.57	2.71	3.19	0.48	0.03
10H-5	55.03	55.04	22.63	2.71	3.06	0.35	0.03
11H-2	60.53	60.54	11.73	1.41	1.74	0.33	0.03
11H-7	66.92	66.93	17.99	2.16	2.32	0.16	0.01
13H-1	75.11	75.12	6.04	0.72	0.99	0.27	0.02
14H-2	85.63	85.64	15.45	1.85	2.09	0.24	0.02
14H-6	91.19	91.20	14.25	1.71	1.85	0.14	0.02
15H-2	95.39	95.40	21.59	2.59	3.00	0.41	0.04
15H-5	99.53	99.54	23.40	2.81	3.29	0.48	0.04
17H-1	106.93	106.94	18.50	2.22	2.68	0.46	0.03
17H-5	112.43	112.44	4.42	0.53	0.62	0.09	0.01
18H-3	118.67	118.68	5.96	0.72	0.93	0.22	0.01
18H-7	124.59	124.60	14.99	1.80	2.11	0.31	0.02
19H-3	128.22	128.23	13.44	1.61	1.95	0.34	0.03
20H-4	134.39	134.40	12.22	1.47	1.67	0.20	0.01
21H-1	137.70	137.71	19.69	2.36	2.73	0.37	0.03
21H-5	142.79	142.80	12.96	1.55	1.80	0.25	0.02
22H-1	147.25	147.26	13.34	1.60	1.79	0.19	0.02
22H-7	155.03	155.04	19.51	2.34	2.78	0.44	0.04
23H-2	157.96	157.97	24.10	2.89	3.17	0.28	0.02
23H-7	164.08	164.09	20.09	2.41	2.78	0.37	0.03
24H-2	166.97	166.98	32.86	3.94	4.37	0.43	0.03
24H-6	173.12	173.14	24.57	2.95	3.37	0.42	0.03
25H-2	176.64	176.65	33.94	4.07	4.44	0.37	0.03
25H-6	182.20	182.21	27.03	3.24	3.71	0.47	0.03
26H-2	185.95	185.96	8.22	0.99	1.22	0.23	0.01
26H-7	193.58	193.59	8.11	0.97	1.14	0.17	0.01
27H-1	194.12	194.13	5.09	0.61	0.78	0.17	0.01
28H-2	204.99	205.00	13.22	1.59	1.86	0.27	0.02
28H-6	210.65	210.66	2.87	0.34	0.38	0.04	BD
340-U1400C-							
10H-1	79.30	79.31	7.64	0.92	1.23	0.31	0.01
11H-1	85.96	85.97	17.27	2.07	2.62	0.55	0.02
12H-2	95.55	95.56	13.55	1.62	1.98	0.36	0.02
13H-6	110.90	110.91	15.28	1.83	2.40	0.57	0.03
22H-4	186.42	186.43	9.01	1.08	1.43	0.35	BD
27X-2	227.76	227.77	7.13	0.86	1.34	0.49	0.01
28X-1	235.42	235.43	5.75	0.69	1.01	0.32	BD
29X-2	246.50	246.51	17.93	2.15	2.81	0.66	0.03
30X-1	254.41	254.42	22.03	2.64	3.18	0.54	0.02
31X-1	263.91	263.92	10.65	1.28	1.64	0.36	0.01
32X-3	277.52	277.53	25.32	3.04	3.83	0.79	0.03
33X-3	286.23	286.24	23.12	2.77	3.47	0.70	0.02
35X-3	295.99	296.00	16.47	1.98	2.63	0.65	0.02
36X-2	304.73	304.74	21.04	2.52	3.02	0.50	0.01
37X-2	313.43	313.44	19.09	2.29	3.01	0.72	0.03
38X-1	322.01	322.02	29.04	3.48	4.26	0.78	0.04
38X-6	329.38	329.39	6.95	0.83	1.16	0.33	0.01
39X-2	332.77	332.78	21.48	2.58	3.18	0.60	0.02
40X-1	341.04	341.05	7.00	0.84	1.18	0.34	BD
41X-1	350.85	350.86	22.56	2.70	3.37	0.67	0.03
42X-2	361.46	361.47	7.67	0.92	1.21	0.29	BD
43X-1	369.36	369.37	8.95	1.07	1.39	0.32	BD
44X-2	380.57	380.58	15.96	1.91	2.26	0.35	0.01
45X-4	392.95	392.96	13.08	1.57	2.05	0.48	0.01

Table T2 (continued).

Core, section	Depth (mbsf) Top	Depth (mbsf) Bottom	Carbon (wt%) $CaCO_3$	Carbon (wt%) Inorganic	Carbon (wt%) Total	Carbon (wt%) Organic	Nitrogen (wt%)
46X-1	397.95	397.96	14.72	1.77	2.26	0.50	0.02
47X-1	407.85	407.86	19.80	2.37	2.87	0.50	0.02
48X-CC	417.46	417.47	31.71	3.80	4.61	0.81	0.03
49X-1	427.01	427.02	24.92	2.99	3.75	0.76	0.03

BD = below detection, values reported as 0.

Table T3. Composition of interstitial pore water, Site U1400.

Core, section	Depth (mbsf) Top	Depth (mbsf) Bottom	Alkalinity (mM)	pH	Cl (mM)	±	Salinity	NH_4 (mM)	Na (mM)	±	Mg (mM)	±	K (mM)	±	Ca (mM)	±	ΣS (mM)	±
340-U1400B-																		
7H-4	31.24	31.34	3.40	7.57	561.9	1.4	37	0.02	471	6	52.8	0.3	11.0	0.1	10.47	0.10	27.9	0.1
8H-5	42.40	42.50	3.48	7.53	560.0	1.8	37	0.02	468	3	52.5	0.5	10.8	0.1	10.42	0.09	27.9	0.4
9H-1	45.90	46.00	3.64	7.46	559.9	3.8	37	0.03	473	3	52.7	0.5	10.8	0.2	10.67	0.08	28.0	0.3
10H-3	52.91	53.01	3.92	7.38	559.6	3.5	37	0.10	474	3	52.7	0.4	10.9	0.2	10.79	0.05	27.9	0.2
10H-6	57.42	57.52	4.20	7.38	559.3	0.0	37	0.21	470	4	51.8	0.6	10.6	0.2	10.49	0.10	27.4	0.3
11H-4	63.92	64.02	4.32	7.47	562.9	1.5	37	0.24	473	3	52.2	0.7	10.8	0.1	10.46	0.13	27.2	0.3
12H-2	70.08	70.18	4.09	7.52	560.9	2.2	37	0.13	473	3	52.7	0.5	10.7	0.2	10.75	0.07	27.9	0.3
13H-5	81.40	81.50	5.01	7.56	564.9	2.4	37	0.48	476	3	52.4	0.4	10.2	0.2	9.98	0.09	26.7	0.2
14H-3	87.85	87.95	5.56	7.41	567.6	4.1	37	0.59	478	3	52.1	0.4	9.9	0.1	9.32	0.06	25.6	0.2
15H-4	98.80	98.90	5.68	7.41	569.0	1.2	37	0.60	479	1	52.4	0.4	9.6	0.1	9.45	0.05	25.1	0.3
17H-4	111.53	111.63	5.77	7.45	568.5	3.3	37	0.64	477	2	52.7	0.4	9.6	0.2	9.75	0.05	25.5	0.2
18H-4	121.00	121.10	5.77	7.45	565.4	4.5	38	0.65	479	1	52.7	0.4	9.3	0.3	9.88	0.05	25.7	0.3
19H-2	127.52	127.62	5.80	7.49	571.3		37	0.62	478	2	53.8	0.4	9.1	0.2	9.97	0.05	25.7	0.4
20H-3	133.21	133.31	5.85	7.45	572.2		37	0.65	477	0	52.8	0.4	9.2	0.1	9.85	0.04	25.4	0.0
21H-5	143.82	143.92	5.85	7.58	570.9	1.3	37	0.68	476	2	52.7	0.4	8.9	0.3	9.73	0.11	25.5	0.3
22H-4	151.83	151.93	5.93	7.49	569.8		37	0.69	478	3	52.6	0.4	9.1	0.2	9.65	0.08	25.3	0.2
23H-4	161.35	161.45	5.81	7.46	568.2	0.3	37	0.68	476	2	52.4	0.4	8.9	0.1	9.71	0.06	25.1	0.2
24H-4	170.88	170.98	5.86	7.43	570.3		37	0.66	477	3	53.0	0.4	8.7	0.0	9.92	0.07	25.2	0.2
25H-4	180.34	180.44	5.51	7.39	570.5		37	0.61	474	3	52.8	0.4	8.4	0.2	9.98	0.07	25.0	0.3
26H-4	189.78	189.88	5.90	7.47	572.9		37	0.67	477	2	52.4	0.5	9.0	0.2	10.19	0.06	25.7	0.3
27H-5	200.79	200.89			569.2		38	0.68	475	3	52.2	0.5	9.2	0.1	10.15	0.09	25.3	0.3
28H-3	207.30	207.40	5.96	7.39	568.8		37	0.66	480	3	52.9	0.5	9.3	0.3	10.22	0.08	25.4	0.3
340-U1400C-																		
27X-4	231.20	231.30	5.86	7.81	570.8		38	0.62	473	4	52.4	0.5	8.9	0.2	10.60	0.10	25.9	0.3
29X-2	247.40	247.50	6.05	7.48	570.8		38	0.64	475	4	52.8	0.4	8.8	0.1	10.46	0.09	25.4	0.2
30X-2	257.00	257.10	6.22	7.39	572.2		38	0.69	478	2	52.4	0.4	9.0	0.1	10.38	0.08	25.1	0.3
31X-3	268.10	268.20	6.52	7.42	569.7		38	0.70	475	4	51.9	0.4	8.8	0.3	10.36	0.09	24.6	0.0
32X-2	276.20	276.30	6.82	7.39	570.3		37	0.73	476	3	51.6	0.4	8.8	0.2	10.29	0.05	24.1	0.3
33X-2	285.80	285.90	6.61	7.28	570.6		37	0.72	476	5	51.6	0.7	8.4	0.1	10.25	0.12	23.3	0.3
35X-4	298.40	298.50	6.38	7.29	568.7		37	0.70	473	2	51.9	0.5	8.1	0.2	10.30	0.05	23.9	0.3
36X-3	306.50	306.60	6.48	7.33	569.8		37	0.73	474	2	51.4	0.4	8.3	0.2	10.25	0.05	23.6	0.3
37X-1	313.12	313.22	6.72	7.36	567.5	3.2	37	0.74	475	2	51.7	0.4	8.4	0.2	10.46	0.07	23.7	0.4
38X-5	328.30	328.40	6.88	7.37	569.2	3.3	38	0.74	475	0	51.4	0.1	8.4	0.1	10.68	0.00	23.9	0.0
39X-5	337.71	337.81	6.75	7.46	568.2		38	0.73	477	2	52.0	0.5	8.5	0.2	10.95	0.06	24.7	0.2
40X-1	341.50	341.60	6.15	7.42	568.2		38	0.72	476	4	52.1	0.7	8.2	0.1	10.78	0.10	24.7	0.3
41X-1	351.10	351.20	6.06	7.39	566.0		37	0.61	472	3	52.5	0.5	7.4	0.0	10.90	0.15	23.7	0.1
42X-2	362.20	362.30	6.54	7.44	570.1		37	0.68	478	6	51.7	0.6	8.2	0.1	11.00	0.17	23.5	0.0
44X-1	379.75	379.85	6.40	7.34	570.4		37	0.68	476	5	50.8	0.5	8.0	0.0	11.56	0.20	22.9	0.2
45X-3	392.45	392.55	6.04	7.35	568.6		37	0.68	477	4	50.6	0.6	8.0	0.0	12.82	0.23	23.3	0.3
49X-1	427.48	427.58	4.76	7.25	560.2		37	0.57	465	5	47.8	0.9	6.7	0.0	14.78	0.39	18.1	0.2

Uncertainties represent ±1σ based on repeat analyses for Cl. Shaded samples represent average values for Na, Mg, K, Ca, and ΣS (total sulfur) from duplicate analyses from separate runs. Samples in italics represent averages from within-run duplicates.

Table T4. Correlation point picks and depth shifts, Hole U1400C.

Original depth (mbsf)	Corrected depth (mbsf)	Difference (m)
17.675	20.099	–2.424
21.394	25.202	–3.808
22.660	26.021	–3.360
30.471	33.143	–2.672
32.796	34.412	–1.616
40.598	37.373	3.226
43.809	38.720	5.089
49.974	41.351	8.623
50.853	42.805	8.048
53.584	45.039	8.546
58.912	48.065	10.847
62.297	51.039	11.257
64.330	52.947	11.383
65.714	54.474	11.240
66.812	55.775	11.036
70.007	58.712	11.295
72.448	62.254	10.195
81.728	68.940	12.788
84.202	70.508	13.694
87.283	75.310	11.973
89.885	78.342	11.543
91.579	79.397	12.182
94.686	84.313	10.373
100.163	90.056	10.107
102.785	92.640	10.146
105.685	95.663	10.022
108.267	98.641	9.626
109.504	99.839	9.664
111.657	101.132	10.525
112.497	101.738	10.759
114.467	105.313	9.154
117.697	107.228	10.469
120.439	109.275	11.164
124.668	111.863	12.804
131.016	115.720	15.296
135.347	119.865	15.482
138.761	122.855	15.906
141.917	125.640	16.276
143.242	127.161	16.080
145.226	131.195	14.031
151.142	136.243	14.899
155.890	140.774	15.116
160.360	145.382	14.978
164.141	149.990	14.152
166.534	152.332	14.202
167.471	153.292	14.179
171.544	157.606	13.938
173.258	160.118	13.141
177.453	163.010	14.443
182.578	166.778	15.800
216.066	190.624	25.441
233.332	195.951	37.381